Concentrated plasticity modeling of RC frames in time-history analyses

Authors

Eleonora Bruschi[(a)]; Paolo M. Calvi[(b)]; Virginio Quaglini[(a)]

Affiliation:

[(a)] Politecnico di Milano, Department of Architecture, Built Environment and Construction Engineering, Piazza Leonardo da Vinci 32, 20133 Milan, Italy;

[(b)] University of Washington, More Hall, Department of Civil and Environmental Engineering, Seattle, WA 98195, USA;

e-mail address:

eleonora.bruschi@polimi.it ; pmc85@uw.edu ; virginio.quaglini@polimi.it

Corresponding Author

Virginio Quaglini, MSc, PhD

Politecnico di Milano, Department of Architecture, Built Environment and Construction Engineering, Piazza Leonardo da Vinci 32, 20133 Milan, Italy

e-mail: virginio.quaglini@polimi.it

Abstract

The study aims at giving an insight into the effects of modelling decisions that are adopted in concentrated plasticity formulations used in time history analyses to model the behavior of reinforced concrete frames, by investigating the sensitivity of the estimated structural response on the assumed length of the plastic hinge region L_{pl} and the effective area moment of inertia I_{eq} of the cracked concrete section. Four frames with 2, 4, 8 and 12 stories, designed in accordance with the Italian Building Code and characterized by a flexural behavior, are taken as case-studies. Structural models are coded in the OpenSees framework adopting various formulations of L_{pl} and I_{eq} taken both from the literature and the European and the Italian codes. The results of the analyses are compared to the ones provided by a distributed plasticity formulation and evaluated considering engineering demand parameters such as internal forces and deformations, and absolute accelerations. The main differences between the predictions provided from the distributed and the lumped inelasticity approaches regard the estimates of the inter-story drift ratio and the maximum base moment, while predictions of absolute acceleration and maximum base shear are found to be more consistent; a certain influence of the number of stories is also highlighted. Eventually, the agreement between concentrated and distributed plasticity formulations can be improved by adopting an effective area moment of inertia of concrete cracked section dependent on the axial load in the structural member.

Keywords

Reinforced concrete frame; plastic hinge length; effective area moment of inertia; concentrated plasticity; concrete cracking; time history analyses; forceBeamColumn element object; design codes.

1. Introduction

Static (Pushover) and dynamic (Time History) non-linear analyses are used in design practice to assess the seismic vulnerability of reinforced concrete (RC) buildings. The analyses are performed using Finite Element Models (FEMs), and various software programs for structural calculation, like e.g., OpenSees [1], Abaqus [2], MidasGen [3] and SAP2000 [4] are available to the designers. Considering the structural non-linear response, there are two major sources of non-linearity, namely material and geometric non-linearity. Material non-linearity is considered the primary source of damage for low- and medium-rise building structures, while geometrical non-linearities should be accounted for in high-rise buildings with small aspect ratios subjected to large horizontal deflections that introduce P-Delta effects. For the non-linear material response, the Finite Element simulation falls into two main categories, namely distributed plasticity models and concentrated (or lumped) plasticity models

Concentrated plasticity formulations are easier to implement, computationally more effective and are able to provide fairly accurate and reliable predictions in most practical situations [5], [6]. There are different levels of complexity that can be taken into account to address material non-linearities. For instance, the length of a structural member affected by anelastic behavior can be represented either by means of a single rotational spring with assigned non-linear moment-curvature relationships, or by an element made of non-linear fiber sections [7]. Two important modelling decisions that have been shown to affect the accuracy of the model indeed concern: (i) the "plastic hinge length" (L_{pl}), a fictious length related with the extension of the part of a structural member over which non-linear behavior is activated; and (ii) the flexural stiffness of the cracked concrete section, which is generally taken into account by introducing an artificially low effective area moment of inertia (I_{eq}).

Several plastic hinge length formulations have been proposed in the literature (e.g., [8]-[21]) and later incorporated in seismic codes and guidelines (among the others, e.g., FEMA 356 [22], ACI 318 [23], Eurocode Part 8 [24] and, with reference to the Italian scenario, the Explanatory Circular to the Italian

Building Code [25]). To the Authors' knowledge, a comparative evaluation of concentrated plasticity models for non-linear dynamic analyses of RC structures has not been conducted yet, and the choice is ultimately left to the structural engineer. However, not negligible differences exist among the various formulations, which can lead to inconsistent approaches and possibly conflicting results, see e.g., references [26], [27].

In the same way, though cracking is noted to reduce the stiffness of RC members and it should be accounted for in numerical models [28]-[30], a common approach is missing. Modelling strategies based on the use of a reduced area moment of inertia with respect to the one of the gross cross-section have some merit [24] [25] [31] [32], but the coefficients of reduction coefficients proposed in the codes are mainly empirical rather than based on rigorous studies [33].

The present work aims at giving guidance to structural engineers who perform non-linear dynamic analyses on RC frames, by providing some insight into the effects of the modelling decisions on the plastic hinge length and the reduction of the area moment of inertia in lumped plasticity formulations. The paper does not intend to provide an overview of all the available modelling choices for plasticity of RC columns and beams, but it focuses on modelling of structural elements where the non-linear behavior is activated at the end regions, while in the middle the behavior remains elastic.

The State of Art describes the significance and the hypotheses at the basis of the plastic hinge length formulation and provides a critical discussion of the various expressions proposed in research works and in the European and the Italian norms; some expressions for the effective area moment of inertia I_{eq} of cracked concrete section are presented and discussed as well.

A numerical investigation conducted on a set of four case-study RC frames is performed focusing on the effects of the modelling decisions. The structures, designed in compliance with the current code recommendations, are characterized by a flexural behavior and are respectful of the principles of the capacity design. Every structure has been modelled according to both distributed and concentrated plasticity formulations, and in each of them the inelasticity is defined at the sectional level, assigning

a material uniaxial inelastic behavior to concrete and steel. The distributed plasticity models, where plasticity can spread across the whole length of each structural members, are expected to be able to capture the overall flexural behavior of the case-study frames [34]-[36], and therefore are assumed as the benchmark. Several concentrated plasticity models are formulated accounting for different expressions of the plastic hinge length L_{pl} and the effective area moment of inertia taken from the literature and the European and Italian norms. Non-linear time histories are performed according to the provisions of the Italian Code [37], and the models are compared in terms of predicted structural drifts and accelerations, and reactions (forces and moments) at the base, which are the engineering demand parameters usually considered for the verification of RC structures.

2. Review of the State of Art

In an RC frame designed according to capacity design principles, during a seismic event, plastic flexural mechanisms are expected to be activated at the end sections of the beams and at the basis of the columns of the first floor [14]. These dissipative zones, where non-linear mechanisms such as yielding of the longitudinal reinforcement, extensive spalling of concrete cover, diagonal cracking and crushing of concrete core, and buckling and fracture of longitudinal steel bars are engaged [38], represent the so-called *real* plastic hinge regions, also termed as *critical zones* in the Eurocode [24]. The curvature distribution inside the critical zones is very complex and case-dependent, as it is affected by the concrete compressive strength, the bottom/top reinforcement ratio, the transverse reinforcement ratio and the shear span to depth ratio [38] [39], and the maximum curvature may do not occur in the same section where the moment has its maximum [19].

In the framework of non-linear analyses, this complex behavior can be represented with fair accuracy by means of a concentrated plasticity formulation, i.e. assuming that the structure is composed of beam–column members made of an elastic core and "plastic hinges" of assigned length at both ends, where the plastic behavior can be activated. The concept of the plastic hinge length was initially introduced by Park and Paulay [40] who considered a cantilevered RC column subjected to a transversal force, and determined the ultimate top displacement according to the expression:

$$\delta = \frac{\varphi_y z^2}{3} + (\varphi_u - \varphi_y) L_{pl} (z - 0.5 L_{pl}) \quad (1)$$

where z is the shear span of the column, φ_u is the ultimate curvature at failure and φ_y is the curvature at yielding. Within this simplification, which is rigorously valid only for members characterized by a purely flexural behavior, the plastic hinge length (L_{pl}) does not correspond to the actual length of the critical zone over which the inelastic deformation actually spreads, but is instead the *effective* length [31] over which a given plastic curvature is assumed to be constant and is integrated to calculate the effective chord rotation, including shear and fixed-end rotation contributions, under the Bernoulli's

plane section assumption [41], [42]. All the analytical models developed after Park and Paulay are based on this fundamental hypothesis ([14]-[19]). Fardis [16] introduced an additional contribution to Eq. (1), representing the fixed-end rotation due to the slippage of the longitudinal bars from the anchorage zone $a_{sl}(\theta_{u,slip} - \theta_{y,slip})$, where $a_{sl} = 0$ when the slippage is not physically possible and $a_{sl} = 1$ otherwise, and $\theta_{u,slip}, \theta_{y,slip}$ are the rotations due to slippage at failure and at yielding, respectively.

Several studies have been conducted to formulate plastic hinge length expressions suitable for beams and columns, and a comprehensive list is reported in Table 1.

Reference	*Plastic Hinge Length (L_{pl})*	*Element applicability*
Baker, 1956[8]	$k_1 k_2 k_3 \left(\frac{z}{d}\right)^{1/4} d$	beams and columns
Mattock, 1964[9]	$\frac{d}{2}\left[1+\left(1.14\sqrt{\frac{z}{d}}-1\right)\left\{1-\left(\frac{q-q'}{q_b}\right)\sqrt{\frac{d}{16.2}}\right\}\right]$	beams
Sawyer, 1964[10]	$0.25d + 0.075z$	beams
Corley, 1966[11]	$0.5d + 0.2\sqrt{d}\left(\frac{z}{d}\right)$	beams
Mattok, 1967[12]	$0.5d + 0.05z$	beams
Priestley et al., 1987[13]	$0.08z + 6d_b$	columns
Paulay et al., 1992[14]	$0.08z + 0.022 d_b f_y$	beams and columns
Panagiotakos et al., 2001[15]	$0.12z + 0.014 a_{sl} d_b f_y$	beams and columns
Fardis, 2007[16]	$0.09z + 0.2h$	beams and columns
Priestley et al., 2007[17]	$0.2(\frac{f_u}{f_y}-1)z + 0.022 d_b f_y$	beams and columns
Bae et al., 2008[18]	$\left\{\left[0.3\left(\frac{P}{P_0}\right)+3\left(\frac{A_s}{A_g}\right)-0.1\right]\left(\frac{z}{h}\right)+0.25\right\}h \geq 0.25h$	Columns
Elmenshawi et al., 2012[19]	$\left[0.08z + 0.022 d_b f_y + l_s\right]$	beams and columns
Mortezaei et al., 2013[20]	for far-fault earthquakes: $\left\{\left[0.4\left(\frac{P}{P_0}\right)+3\left(\frac{A_s}{A_g}\right)-0.1\right]\left(\frac{z}{h}\right)+0.6\right\}h \geq 0.6h$ for near-fault earthquakes: $\left\{\left[0.4\left(\frac{P}{P_0}\right)+3\left(\frac{A_s}{A_g}\right)-0.1\right]\left(\frac{z}{h}\right)+0.45\right\}h \geq 0.45h$	Columns
Ning et al., 2016[21]	$z\left(0.042+0.072\frac{P}{P_0}\right)+0.298h+6.407d_b$	Columns

Table 1: Plastic Hinge Length formulations proposed the literature

The expressions in Table 1 were mainly developed upon experimental investigations conducted on beam and column members subjected to monotonic and cyclic loading, and only in few cases the estimation of L_{pl} was based on numerical simulations [20] [43].

In two independent studies, Bae and Bayrak [18] and Elmenshawi et al. [19] compared experimental plastic hinge lengths, determined either as the measured length of an extensively damaged zone or as

a mathematical expression relating the experimental curvature to the relevant chord displacement, with analytical models from the literature [8]-[15]. The large scatter of results and the different performances of the models that were observed were ascribed to the fact that each formulation relies on particular assumptions, including the position of the actual hinge, i.e. of the center of rotation in the plastic hinge model, the definition of yielding and ultimate curvatures, the section geometry, the constitutive behavior of materials, the transverse reinforcement, the support conditions and the magnitude and type of loading [20], which are not the same for all the models. Moreover, the assessed models give different weight to the various anelastic mechanisms, which makes the dependence on a particular parameter predominant over the others.

Because the length of the zone affected by non-linear behavior tends to be greater for beams than for columns, dedicated theoretical expressions were proposed. The greater plastic hinge length observed for beams is attributed indeed to the low axial forces they are normally subjected to, which makes them more prone to shear-induced flexural deformations [19]. Further to this, beams are usually characterized by an asymmetric reinforcement layout. This feature affects the plastic hinge length too.

In the early models [8]-[12], expressions for L_{pl} accounted for bending deformations only. In a first improvement, Priestley and Park [13] proposed a two-component formulation, where the first term accounts for column bending, while the second term accounts for the fixed–end rotation due to bar slip and yield penetration of longitudinal bars into the column base. Paulay and Priestley [14] postulated the dependency of L_{pl} on the yield strength f_y of the longitudinal reinforcement, to more accurately account for different grades of flexural reinforcement, and later Priestley et al. [17] emphasized the importance of the ratio of ultimate tensile strength to yield strength of steel f_u/f_y; for low f_u/f_y ratios plasticity is indeed activated close to the end section of the RC member, resulting in a short plastic hinge length, whereas high f_u/f_y ratios increase the length of spread of plasticity across the RC member.

Panagiotakos and Fardis [15] reviewed a large number of tests embracing both cantilevered columns and supported beams. The geometry of the tested specimens, the amount and layout of the reinforcement, the concrete strength, the type of steel, and the axial load covered a very large range of options. On such basis, the Authors proposed an expression where L_{pl} still depends on the shear span z, the diameter of the reinforcement d_b and the yield strength of steel f_y, but increased the weight of the flexural contribution and reduced the weight of the reinforcement.

Bae and Bayrak [18] formulated a new expression for L_{pl} that included the dependence on the amount of longitudinal reinforcement through the ratio $\frac{A_s}{A_g}$ (where A_g is the gross area of concrete section and A_s is the area of tension reinforcement), because they observed that L_{pl} has a consistent tendency to increase proportionally to this quantity, independently of the axial load. This behavior was confirmed in later studies [20] [43]. Furthermore, by testing column specimens subjected to a wide range of axial load, Bae and Bayrak [18] concluded that L_{pl} is nearly constant at low load levels but, beyond a certain threshold, namely $P = 0.2\ P_0$, where P is the applied axial force, and P_0 is the nominal axial load capacity, it increases significantly with increasing of the compression.

Elmenshawi et al. [19] introduced the contribution of the "shear spread" length l_s, which is more significant in beams than in columns because shear effects are normally more critical in flexural elements subjected to low axial force, where the contribution of the concrete in resisting shear stresses can be disregarded.

Ameli and Pantelides [44] proposed an iterative procedure to determine L_{pl} for either cast-in-place or precast columns, capable of simulating both the local and the global experimental response. The proposed expressions of L_{pl} accounted for both low-cycle fatigue and bond-slip and were in good agreement with empirical expressions available in literature, like e.g., in references [13] and [15].

Recently, Pereira and Romão [38] highlighted the need to consider all the local mechanisms that take place in the critical zone, in order to properly quantify the damage localization length; in fact, before the yielding of the reinforcement, the interface effects, along with flexure and shear deformations,

mainly contribute to the deformation capacity, while, after yielding, the behavior is predominantly governed by flexure. For this reason, the authors suggested to decouple the interface effects from the material strain level in order to formulate these mechanisms in terms of the size-dependent behavior of the constitutive materials at their ultimate state, namely the strength and the stiffness deterioration of the concrete and reinforcing steel compressive and tensile responses.

It is worth mentioning that factors affecting the plastic hinge length in RC elements subjected to monotonic loadings could be different than those under reversed loading (either static or dynamic) [19], and therefore some expressions (e.g., references [15] and [16]) reported in Table 1 are valid under cyclic loading only.

Based on a wide experimental and numerical background, recommendations for concentrated plasticity modelling of flexural RC members in non-linear analyses were introduced in the Eurocode 8 (for brevity EC8) for design of seismic resistant structures. Part 2 of EC8 [45] gives provisions for modelling of RC piles of bridges, while Part 3 [24] addresses general modelling issues of RC members of framed buildings. Specifically, the Code [24] provides two formulas for the plastic hinge length

$$L_{pl} = 0.1z + 0.17h + 0.24\left(\frac{d_b f_y}{\sqrt{f_c}}\right) \tag{2}$$

$$L_{pl} = \frac{z}{30} + 0.2h + 0.11\left(\frac{d_b f_y}{\sqrt{f_c}}\right) \tag{3}$$

Both formulations are valid under the assumptions of the curvature profile across the member length given by Eq. (1), and the yield and ultimate rotations determined in accordance with Park and Paulay [40]. The Code recommends to use formula (2) in combination with a confinement model for concrete in accordance with Eurocode 2 [46], with the stress-strain relationship defined by a parabolic-rectangular curve according to the stress block theory; on the contrary, the formula (3) is valid when a more refined stress-strain model representing the improvement of φ_u with confinement under cyclic loading is assumed:

$$f_{cc} = f_c[1 + 3.7\left(\frac{\alpha_c \rho_{sx} f_y}{f_c}\right)^{0.86} \tag{4}$$

$$\varepsilon_{cc} = \varepsilon_{c2}\left[1 + 5\left(\frac{f_{cc}}{f_c} - 1\right)\right] \tag{5}$$

$$\varepsilon_{cu} = 0.004 + 0.5\frac{\alpha_c \rho_{sx} f_y}{f_c} \tag{6}$$

where f_{cc} is the confined concrete strength and ε_{cc} is the associated strain, ε_{cu} is the ultimate strain of the extreme fiber of the compression zone, ρ_{sx} is the ratio of transverse steel parallel to the direction of loading and α_c is the confinement effectiveness factor, which depends on the dimension of the confined core and the stirrup spacing.

Both expressions of Eq. (2) and Eq. (3) include the contributions of the shear span z, the overall depth h of beam or column cross-section, the diameter d_b and the yield strength f_y of the longitudinal reinforcement, and the concrete compressive strength f_c. It is noteworthy that only few equations, namely those defined in references [8] [18] [20] [21], among those reported in Table 1 account for f_c, since experimental findings reported in literature seem to suggest that RC members made of high strength concrete (up to 175 MPa) have comparable extension of the plastic region with their normal strength concrete counterparts [19]. However, the concrete strength may have an indirect influence on L_{pl}, as shown, e.g., in reference [43], as it affects the curvature distribution and the flexural strength and, in turn, the shear demand on the element, which is considered (alongside the cross-section effective depth) the main factor influencing the plastic hinge length.

By referring to the Italian scenario, the Italian Building Code "Technical Norm for Constructions" (for brevity NTC) [37], in its Explanatory Circular [25] provides the same expression of L_{pl} as in Eq. (2), but differently from EC8 [24], it suggests to adopt the detailed stress-strain model for confined concrete according to Mander [47], instead of the parabolic-rectangular relationship defined in Eurocode 2 [46]. The effect of this combination will be investigated later.

In the concentrated plasticity formulation, the inelastic behavior is activated only within assigned regions of the structural member, while the remaining part is assumed to behave elastically. In order

to account for the reduced flexural stiffness, an effective area moment of inertia I_{eq} of the elastic region intended to mimic (in a simplified manner) cracking-induced softening phenomena is frequently adopted [28]-[30]. The simplest approach consists in taking the effective area moment of inertia as an assigned fraction of the area moment of inertia I_g of the gross cross-section, where 50% of I_g is a common figure [28] [29]. In contrast, other authors suggest to adjust the effective stiffness on a mechanical model. Brason and Metz [48] proposed an expression for I_{eq} that accounts for the gradual change in stiffness with the progression of cracking

$$If\ M_b > M_{cr}, then\ \ I_{eq} = \left(\frac{M_{cr}}{M_b}\right)^3 I_g + \left[1 - \left(\frac{M_{cr}}{M_b}\right)^3\right] I_{cr},\ with\ I_{eq} \leq I_g \tag{7a}$$

$$If\ M_b \leq M_{cr}, \qquad then\ I_{eq} = I_g \tag{7b}$$

where M_b is the bending moment acting on the concrete section, M_{cr} is the bending moment at first cracking and I_{cr} is the area moment of inertia of the cracked section evaluated at the critical point of the moment-curvature relationship. Fardis [16] proposed both a *theoretical effective stiffness*, calculated directly from the yield moment M_y and the chord rotation at yielding θ_y, and an *empirical effective stiffness*, fitted directly to test results. This latter expression depends on the structural member under consideration, the possible slippage of the longitudinal bars from their anchorage beyond the member end section, the shear span to depth ratio $(\frac{z}{h})$ and the axial load ratio $\nu = \frac{N}{A_g f_c}$ (here N is the axial load under gravity actions alone):

$$E_c I_{eq} = \alpha(0.8 + \log_{10}\frac{z}{h})\left(1 + 0.048 \min\left(\frac{N}{A_g}, 50MPa\right)\right)(1 - 0.25a_{sl})E_c I_g \tag{8}$$

where the value of α depends on the member type (i.e., beams, columns, or walls) and a_{sl} counts either 1 or 0 depending on whether slippage of longitudinal steel is possible or not.

Another approach was proposed by Priestley [49], who recommended to calculate the effective flexural stiffness from the bilinear approximation to the moment – curvature relationship, according to the expression:

$$I_{eq} = \frac{M_N}{E_c \varphi_y} \tag{9}$$

where E_c is the concrete modulus of elasticity, M_N is the cross-section nominal flexural strength and φ_y is the yield curvature, which for rectangular columns can be evaluated as $\varphi_y h = 2.12\ \varepsilon_y \pm 10\%$, being ε_y the yield strain of the longitudinal reinforcement and h the cross-section depth [49]. This formula has the merit to take into account the axial force, which increases the nominal flexural strength of the columns at the lower stories of a multistory building, and allows to differentiate between columns and beams. For ease of implementation, in design codes I_{eq} is generally assigned as a fixed fraction of I_g, with only few exceptions, like e.g. the North American code ACI 318 [23] where values of I_{eq} accounting for axial load, eccentricity, reinforcement ratio, and concrete compressive strength, similarly to the moment-dependent expression proposed by Branson and Metz [48], e.g., Equation (7), are adopted. Part 1 of EC8 [50] assigns the flexural and shear stiffnesses of the cracked concrete section as one-half of the stiffnesses of the uncracked section, thus defining the effective area moment of inertia as:

$$I_{eq} = 0.5 I_g \tag{10}$$

and the same provision is given in the Italian Building Code [37]. A similar approach is followed also in e.g., the Greek and the New Zealand codes [31] [32], but the two norms prescribe different reduction factors, ranging from $0.4I_g$ for beams to $0.8I_g$ for the interior columns of a frame, depending on the expected axial load ratio of the RC member under consideration.

3. Numerical investigation

3.1 RC case study frames

The case-study structures examined in the study consist of four RC building frames from two to twelve stories in height. Each floor has three bays of 5 m in both horizontal directions (Figure 1) and a constant inter-story height of 3.5 m. The geometry of the four frames and the material properties are taken from reference [51].

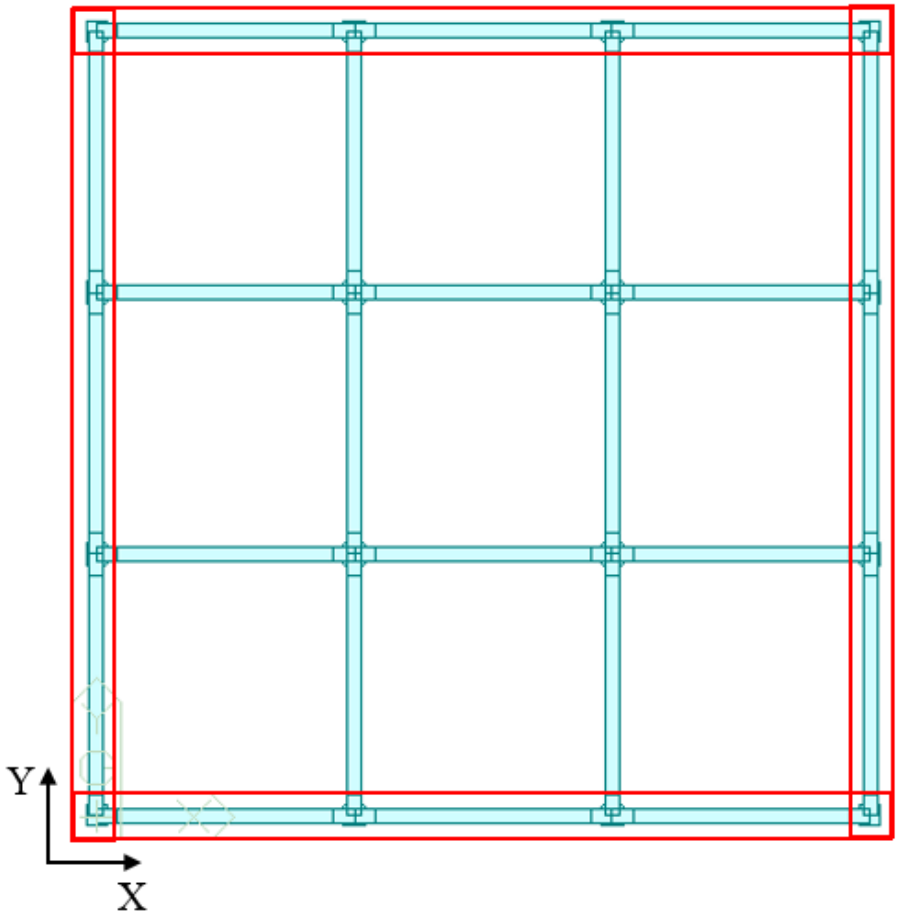

Figure 1: Typical plan of the case-study structures, with highlights of the peripheral seismic resistant frames

The structures can be assumed as paradigmatic of low-rise (2 and 4 stories) and medium-rise (8 and 12 stories) buildings, designed in compliance with the Italian Building Code [37] for medium ductility class (CDB) with a behavioral factor q = 3.5, respecting the strong-column/weak-beam concept. The municipality of L'Aquila (Italy, latitude 13.3944°, longitude 42.366°), a city in a high-seismic prone area (PGA = 4.062 m/s^2) belonging to seismic zone 1 (highest seismic hazard) of the Italian seismic classification [37], with soil Type C (medium-dense sand, gravel or stiff clay formation) and topographic category T_2, is assumed for the design. The buildings are designed as ordinary structures subjected to overcrowding, with functional class cu = II, and an anticipated design life V_n = 50 years. Dead and live load contributions are given in Table 2, where the assumed live load Q = 4 kN/m^2 applies to use category D (shopping areas) of the Code [37]. The seismic combination, calculated according to the recommendations of NTC [37] and taking a combination factor of 0.6 for the live load Q as prescribed for use category D, controlled the design of the buildings.

Level	***G_1*** ***[kN/m^2]***	***G_2*** ***[kN/m^2]***	***Q*** ***[kN/m^2]***
1 to n-1	3.5	4.5	4
n (roof)	3.5	3.5	2.18

Table 2: Dead and live loads (n: number of stories; *G_1*: permanent structural loads; *G_2*: permanent non-structural loads, *Q*: live loads)

The peripheral frames are designed to provide horizontal resistance to seismic loads, while the internal columns are designed to carry only gravity loads (Figure 1). Two-way rigid floor slabs are assumed at each floor.

The frames are designed as ductile RC structures made from slender members, failing in flexure. For this reason, brittle mechanisms, such as shear failure of beams or columns or beam-column joints, are not taken into account in the numerical model. Also, other failure mechanisms like bond slip and low-cycle fatigue are not addressed in the study. In each building, the cross sections of beams and columns

are kept constant for all floors (Table 3), in order to precisely control the locations where plastic hinges are triggered (namely, at the bases of the columns of the first floor and at the ends of the beams of each floor).

	2 stories	*4 stories*	*8 stories*	*12 stories*
Columns	40 x 40	70 x 70	70 x 70	90 x 90
Beams	30 x 40	50 x 60	50 x 70	50 x 90

Table 3: Cross-section dimensions for columns and beams, in [cm]

In accordance with NTC [37], the total longitudinal reinforcement ratio ρ_l of the seismic resistant columns ranges from 1% to 4%, while in beams the ratio of the longitudinal reinforcement in tension, ρ_t, and the ratio of the longitudinal reinforcement in compression, ρ_c, fulfill the condition $\frac{1.4}{f_y} < \rho_t < \rho_c + \frac{3.5}{f_y}$ (Table 4).

Floors	***2 stories***		***4 stories***		***8 stories***		***12 stories***	
	ρ_t	ρ_c	ρ_t	ρ_c	ρ_t	ρ_c	ρ_t	ρ_c
$11^{\text{th}} - 12^{\text{th}}$							0.47	0.47
$9^{\text{th}} - 10^{\text{th}}$							0.59	0.59
$7^{\text{th}} - 8^{\text{th}}$					0.52	0.52	0.71	0.71
$5^{\text{th}} - 6^{\text{th}}$					0.77	0.77	0.82	0.82
$3^{\text{rd}} - 4^{\text{th}}$			1.01	0.76	1.03	1.03	0.94	0.94
$1^{\text{st}} - 2^{\text{nd}}$	1.6	1.26	1.26	1.3	1.03	1.03	1.18	1.18

Table 4: Longitudinal reinforcement ratios in tension and in compression in the critical zones of beams, in [%]

The spacing of transverse reinforcement *s* in the critical zones of the structural members is determined as $s = \min\left\{\frac{B_p}{2}; 17.5cm; 8d_b\right\}$ for seismic resistant pillars, and as $s = \min\{\frac{\zeta}{4}; 225mm; 8 \cdot$

$d_b; 24d_{st}\}$ for beams, where B_p is the section width of the pillars, ζ is the lever arm of the beam cross-section and $d_{st} \geq 6$ mm is the diameter of the stirrups. Table 5 and Table 6 provide the shear reinforcement ratio ρ_{sx} in the critical zones of beams and columns respectively, determined as the ratio $\frac{A_{st}}{Bs}$, where A_{st} is the area of the transverse reinforcement parallel to the direction of horizontal loading and B is the cross-section width of the structural element.

Floors	*2 stories*	*4 stories*	*8 stories*	*12 stories*
$11^{\text{th}} - 12^{\text{th}}$				0.35
$9^{\text{th}} - 10^{\text{th}}$				0.46
$7^{\text{th}} - 8^{\text{th}}$			0.35	0.46
$5^{\text{th}} - 6^{\text{th}}$			0.42	0.56
$3^{\text{rd}} - 4^{\text{th}}$		0.48	0.52	0.56
$1^{\text{st}} - 2^{\text{nd}}$	0.68	0.58	0.52	0.70

Table 5: Shear reinforcement ratio in the critical zones of beams, in [%]

Floors	*2 stories*	*4 stories*	*8 stories*	*12 stories*
all	0.76	0.99	1.42	1.46

Table 6: Shear reinforcement ratio in the critical zones of columns, in [%]

3.2 Numerical model of the RC case study frames

Given the regularity in plan of the examined case-study frames and their symmetry along two horizontal axes, for each building a simplified 2D analysis is conducted on a single external peripheral seismic resistant frame in the X-direction and considering the tributary loads and masses pertaining to this frame, in line with accepted practice [29] [52]. This simplification allows to ease the

interpretation of the results and to focus on the differences observed by using different modelling approaches [28] [29].

Seismic masses were evaluated by taking into account the combination of full permanent loads and live loads as recommended in the Code [37]. The periods of the first and second vibration modes of the frames, associated to more than 85% of the modal mass, are listed in Table 7. The apparently anomalous decrease of the fundamental period observed by switching from the two-story to the four-story frame is however justified by the huge increase of the cross-sections of beams and columns (Table *3*), which results in an overall increase in stiffness for the taller building.

Period [s]	***2 stories***	***4 stories***	***8 stories***	***12 stories***
T_1	0.490	0.433	0.815	0.916
T_2	0.157	0.130	0.262	0.293

Table 7: Elastic periods of the case-study frames

Finite element models of the structures are formulated within the OpenSees framework [1] according to two approaches: distributed plasticity and concentrated plasticity. In the first approach, beams and column members are modeled using the *forceBeamColumn* element object, which is based on the iterative force-based formulation [7]. This element object accounts for three distinct sub-elements, which represent the two external regions and the internal (middle) region of the member, respectively, and permits to assign a different material section model to every sub-element. A two-point Gauss-Radau integration scheme applied to each sub-element is used in the element state determination, for a total of six integration points across the whole element object [7], while geometrical consistency and equilibrium of internal forces between the sub-elements is provided by the object formulation. A variety of combinations of material models, either linear or non-linear, can be used for the external

and the internal regions, encompassing both distributed plasticity and plastic hinge integration. The external regions correspond to the critical zones where non-linear behavior is supposed to be activated [37] and are characterized by closer stirrup spacing, as described in Section 3.1. In these regions, the confined concrete core presents higher compressive strength and ultimate strain than the confined core of sections located in the middle region of the member. A material non-linear fiber section model is formulated in both the external and the middle sub-elements, allowing the spread of the plasticity also beyond the critical zones. Each steel bar is modeled as a single fiber using uniaxial Giuffre-Menegotto-Pinto constitutive law [53], corresponding to *Steel02* material model with isotropic strain hardening [54]. The yield strength f_y, the modulus of elasticity E_s and the strain-hardening ratio b are assumed equal to 390 MPa, 200,000 MPa and 0.01, respectively; the parameters that control the transition from the elastic to the plastic branch are assigned as $R_0 = 18$, $C_{R1} = 0.925$ and C_{R2}= 0.15, as recommended in reference [55]. The concrete part of the cross-section is discretized into 5 fibers in the cover patches and 20 fibers in the core patch. The Mander concrete model [47] is implemented with initial elastic modulus E_c = 29,584 MPa, using the library uniaxial material *Concrete04*, which is based on the model proposed by Popovics [56]. Concrete class is C35/45; the compressive strength of the concrete cover is f_{cover}=35 MPa and strains ε_c and ε_{cu} are 0.002 and 0.004 mm/mm, respectively. Strength and strains of the confined concrete of the core patch are adjusted depending on the reinforcement details of the specific cross-section. The concrete tensile strength and corresponding strain are f_{ct}= 3.67 MPa and ε_t= 0.000124 mm/mm.

In the concentrated plasticity approach, beams and column members are modelled again using the *forceBeamColumn* element [7]; a linear elastic material behavior is assigned to the internal sub-element, whereas the non-linear behavior can be activated only in the two external sub-elements. In these plastic regions, whose length is assigned by the user, the concrete non-linear behavior is modelled through a fiber section model with same material parameters used in the distributed inelasticity formulation, while an effective moment of inertia I_{eq} of the elastic element interior is considered to account for concrete cracking. In this version with elastic interior, the element object is

also known as *beamWithHinges* element object [7] [55]. The same two-point Gauss-Radau integration scheme and the same number of integration points (six across each element object) is therefore used in the element state determination for both distributed and concentrated plasticity representations.

The six expressions of L_{pl} considered in the formulation of the concentrated plasticity models and the supporting hypotheses are listed in Table 8. Each expression for L_{pl} cannot be implemented independently of the paradigms introduced for the curvature profile, method to compute the yield and ultimate curvatures and moments, as well as for the adopted concrete confinement model and type of loading [16] [57]. For this reason, only expressions respectful of the hypotheses of Eq. (1) [40] and valid for both beam and column members have been considered. All the expressions in Table 8 were evaluated considering a well-detailed confinement model [47], and are valid for cycling loading, in line with the scope of the present work. The expressions P-P [14] and NTC (Eq.(2)) [25] can be implemented along with the classical Mander model for confined concrete, while CEN (Eq.(3)) [24], P-F [15] and FAR [16] expressions require the modified Mander formulation described by Eqs.(4) – (6). However, since the concrete strengths evaluated by the two formulations differ by less than 5% and the ultimate strains are nearly equivalent, the classical Mander concrete model has been adopted in the paper whichever the plastic hinge model to be implemented. It must be mentioned that only the ELM expression [19] is not associated to any specific confinement model, but the material and reinforcement properties of the case-study frames are within the range assessed in the experimental tests used for the development of the model [19] and therefore it is assumed that the Manded model can be adopted also for this formulation.

	NTC[25]	CEN[24]
θ_u	$\frac{1}{\gamma_{el}} 0.016(0.3^{\nu}) \left[\frac{\max(0.01;\ \omega')}{\max(0.01;\ \omega)} f_c\right]^{0.225} \left(\frac{z}{h}\right)^{0.35} 25^{\alpha\rho_{sx}\frac{f_{yw}}{f_c}} (1.25^{100\rho_d})$ $\frac{1}{\gamma_{el}}\left(\theta_y + (\varphi_u - \varphi_y) L_{pl}\left(1 - \frac{0.5 L_{pl}}{z}\right)\right)$	$\frac{1}{\gamma_{el}} 0.016(0.3^{\nu}) \left[\frac{\max(0.01;\ \omega')}{\max(0.01;\ \omega)} f_c\right]^{0.225} \left(\frac{z}{h}\right)^{0.35} 25^{\alpha\rho_{sx}\frac{f_{yw}}{f_c}} (1.25^{100\rho_d})$ $\frac{1}{\gamma_{el}}\left(\theta_y + (\varphi_u - \varphi_y) L_{pl}\left(1 - \frac{0.5 L_{pl}}{z}\right)\right)$
θ_y	$\frac{\varphi_y (z + a_v \zeta)}{3} + 0.0013\left(1 + \frac{1.5h}{z}\right) + 0.13\varphi_y d_b f_y / \sqrt{f_c}$	$\frac{\varphi_y (z + a_v \zeta)}{3} + 0.00135\left(1 + \frac{1.5h}{z}\right) + \frac{\varepsilon_y}{d - d'} d_b f_y / 6\sqrt{f_c}$
f_{cc}	$f_c(-1.254 + 2.254\sqrt{1 + \frac{7.94 f_l'}{f_c}} - \frac{2 f_l'}{f_c}$	$f_c(1 + 3.7\left(\frac{\alpha\rho_{sx} f_{yw}}{f_c}\right)^{0.86}$
ε_{cc}	$\varepsilon_{c2}\left[1 + 5\left(\frac{f_{cc}}{f_c} - 1\right)\right]$	$\varepsilon_{c2}\left[1 + 5\left(\frac{f_{cc}}{f_c} - 1\right)\right]$
ε_{cu}	†	$0.004 + 0.5\left(\frac{\alpha\rho_{sx} f_{yw}}{f_{cc}}\right)$
L_{pl}	$0.1z + 0.17h + 0.24 d_b f_y / \sqrt{f_c}$	$\frac{z}{30} + 0.2h + 0.11 d_b f_y / \sqrt{f_c}$

Table 8: Plastic hinge length formulations investigated in the study

	P-P[14]	P-F[15]	FAR[16]	ELM[19]
θ_u	$\left(\varphi_{\mathrm{y}}\frac{z}{3}+(\varphi_u-\varphi_{\mathrm{y}})\mathrm{L_{pl}}\left(1-\frac{0.5\mathrm{L_{pl}}}{z}\right)\right)$	$\left(\varphi_{\mathrm{y}}\frac{z}{3}+(\varphi_u-\varphi_{\mathrm{y}})\mathrm{L_{pl}}\left(1-\frac{0.5\mathrm{L_{pl}}}{z}\right)\right)$	$\theta_y+a_{sl}(\theta_{u,slip}-\theta_{y,slip})+(\varphi_u-\varphi_{\mathrm{y}})\mathrm{L_{pl}}\left(1-\frac{0.5\mathrm{L_{pl}}}{z}\right)$	$\left(\varphi_{\mathrm{y}}\frac{z}{3}+(\varphi_u-\varphi_{\mathrm{y}})\mathrm{L_{pl}}\left(1-\frac{0.5\mathrm{L_{pl}}}{z}\right)\right)$
θ_y	$\left(\varphi_{\mathrm{y}}\frac{z}{3}\right)$	$\varphi_{\mathrm{y}}\frac{z}{3}+0.0025+\frac{a_{sl}(0.25\varepsilon_{\mathrm{y}}\mathrm{d_b}\mathrm{f_y})}{(\mathrm{d}-\mathrm{d}')\sqrt{f_c}}$	$\varphi_{\mathrm{y}}\frac{(z+\mathrm{a_v}\zeta)}{3}+0.0013\left(1+\frac{1.5h}{z}\right)+\frac{a_{sl}(\varphi_{\mathrm{y}}\mathrm{d_b}\mathrm{f_y})}{8\sqrt{f_c}}$	$\left(\varphi_{\mathrm{y}}\frac{z}{3}\right)$
f_{cc}	$f_c(-1.254+2.254\sqrt{1+\frac{7.94f_l'}{f_c}}-\frac{2f_l'}{f_c}$	$f_c(1+3.7\left(\frac{0.5\alpha\rho_s f_{yw}}{f_c}\right)^{0.87}$	$f_c(1+3.7\left(\frac{\alpha\rho_{sx}f_{yw}}{f_c}\right)^{0.86}$	†
ε_{cc}	$0.002\left[1+5\left(\frac{f_{cc}}{f_c}-1\right)\right]$	$0.004+0.6\left(\frac{\varepsilon_{su}\rho_s f_{yw}}{f_{cc}}\right)$	†	†
ε_{cu}	$0.004+1.4\left(\frac{\rho_s f_{yw}\varepsilon_{sm}}{f_{cc}}\right)$	†	$0.0035+\left(\frac{10}{h_c}\right)^2+0.4\left(\frac{\alpha\rho_{sx}f_{yw}}{f_{cc}}\right)$	†
L_{pl}	$0.08z+0.022d_b f_y$	$0.12z+0.014a_{sl}d_b f_y$	$0.09z+0.2h$	$0.08z+0.022d_b f_y+l_s$

† not specified in the reference

Table 8 continued: Plastic hinge length formulations investigated in the study

The flexural area moment of inertia of the interior elastic sub-element was initially reduced by 50% with respect to that of the gross cross-section, , as recommended in both NTC [37] and EC8 [50]. In order to assess the effect of the axial load, which increases the cross-section flexural strength of the columns at the lower stories, additional analyses were performed by considering the expression of the effective area moment of inertia proposed by Priestley [49] as per Eq.(9). The two expressions for I_{eq} will be labelled hereinafter as $I_{0.5I_g}$ (Eq.(10)) and I_P (Eq.(9)), respectively. For each case-study frame a total of 12 analyses was therefore carried out considering the combinations of the six L_{pl}s and the two I_{eq}s.

In all models, the masses of the structural members (beams, columns, and slabs) are concentrated at the nodes, dead and live loads are uniformly distributed on each beam and have been calculated according to the tributary area concept; P-Delta effects are considered in the analysis, while bond slip and low-cycle fatigue effects have been disregarded. The columns at the ground floor have fixed base supports, simulating rigid foundations. The damping of the frame is defined according to the Rayleigh method. However, according to other studies [17] [58]-[61], the damping matrix is computed as a function of the tangent stiffness matrix only, assuming 5% damping ratio [62] [63]. In spite today it is well accepted that the values of damping of RC structures should range between 0.5% and 2% for NLTH analyses [64] [65], a 5% value has been chosen in order to take into account the energy dissipation coming from possible infill panels or other non-modelled non-structural components.

The floor slabs are modeled as rigid diaphragms, by constraining the nodes belonging to the same floor to have the same displacement. As highlighted e.g., in references [27], [52], the interaction between beam elements modeled with fiber sections and the rigid diaphragm may distort the response of the structure, overestimating the moment resistance of the beams. Under the effect of the seismic action, concrete elements tend to crack and because of that, the neutral axis of the RC cross-section undergoes a shift. The rigid diaphragm prevents the movement of the neutral axis, causing fictitious compressive axial forces in the beams, thus overestimating the actual bending moment resistance and

modifying the overall collapse mechanism. To avoid this numerical issue, following Barbagallo et al. [52], an "axial buffer" has been introduced in the FE model. This element, which is assigned through a *zeroLength* element object [66] characterized by a virtually zero axial stiffness and very high stiffnesses in shear and bending, is placed between one end of each beam and the adjacent node belonging to the rigid diaphragm, and it works as an axial release to eliminate the fictitious axial force.

In accordance with NTC [37] and with established practice, non-linear dynamic analyses were performed considering a set of seven natural ground motions selected from the European Ground Motion Database [67] using the computer program REXEL [68]. The seismic inputs agree, in the interval of periods between 0.15 and 2.0 seconds, with the elastic spectrum at 5% equivalent viscous damping ratio defined by the Code [37] for the life-safety limit state (SLV) of an ordinary structure (functional class cu=II) with a nominal life V_n = 50 years, located in L'Aquila, soil type C, category T_2.. The magnitude (Mw) of the seven events was chosen within the interval [5.3 – 7.3], with an epicentral distance (R_{ep}) in the range 0–30 km. Details of the input ground motions are provided in Table 9 and Figure 2.

Waveform ID	***PGA [m/s²]***	***SF [-]***	***t [s]***	***Station ID***	***Earthquake Name***	***Magnitude Mw***	***R_{ep} [km]***
42ya	2.49	1.62	26.52	*ST*8	Ionian	5.8	15
133ya	0.93	4.35	26.42	*ST*33	Friuli	6.0	9
333xa	2.25	1.80	41.86	*ST*121	Alkion	6.6	20
599xa	0.97	4.15	47.17	*ST*223	Umbria Marche	5.7	25
772xa	0.56	7.16	15.16	*ST*223	Umbria Marche	5.3	20
1726ya	2.64	1.53	29.18	*ST*549	Adana	6.3	30
6975ya	0.51	7.93	34.85	*ST*327	Izmit	5.8	26

Table 9: Selected natural ground motions; PGA = Peak Ground Acceleration, SF = Scale Factor, *t* = duration of the earthquake

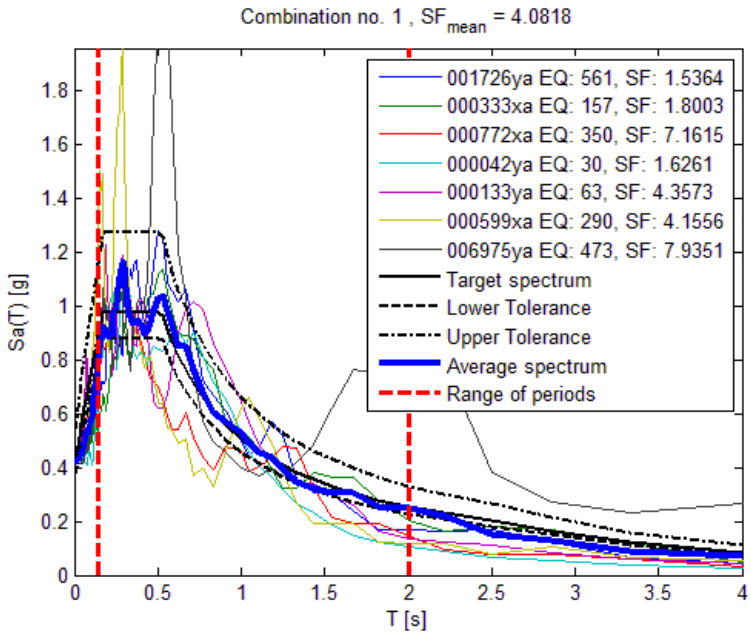

Figure 2: Scaled ground motion spectra and target spectrum according to NTC [37]

Since one of the selected inputs shows an extremely high acceleration peak close to the first periods of the 2-story and the 4-story frames (i.e., 0.490 sec and 0.433 sec, respectively), it was preliminary checked that this record would not induce any irregular behavior of the structures that bias the results. The maximum scatter from the mean estimates was found on the order of either 25% (2-story frame) or 35% (4-story frame) for the inter-story drift, and significantly smaller for the floor accelerations and the internal forces in the columns at the first floor.

4. Results

Since the structures are designed in compliance with the Italian code [37] and respectfully of the principles of the performance-based design, the distributed plasticity formulations (hereinafter referred to as FIBER models) of the four case-study frames are used as the benchmarks. Indeed, in the distributed plasticity model the non-linear behavior is not supposed/intended to be activated in assigned regions of the structural members, but can spread across their whole length, capturing in a more reliable way the overall flexural behavior of the frame [34]-[36]. The concentrated plasticity models have been formulated as coherent and comparable to each other as possible, using expressions of the plastic hinge length L_{pl} respectful of the same fundamental hypotheses, applicable to both beam and column members and valid under cyclic loading. Moreover, these models are consistent with their distributed plasticity counterpart since all of them incorporate the same material properties and constitutive behaviors.

As a first consistency check, plastic deformations were verified to occur in the frames at the same locations independently of the adopted plasticity model. Figure 3 highlights the locations where activation of the plastic hinges has been predicted in time history analyses. Only plastic hinges that are predicted both from the concentrated plasticity formulation of the frame and from the 12 distributed plasticity formulations (resulting from the six L_{pl} and the two I_{eq}) have been reported. Filled spots indicate plastic hinges that are engaged in each model from all ground motions, and empty spots indicate hinges that are engaged in each model by at least two out of the seven ground motions, but not by all of them. The activation of plastic mechanisms at the ends of the beams and at the bases of the ground floor columns is in agreement with the capacity design principles, anticipated in the design of the case-study structures. It is apparent that in each frame, plastic hinges were triggered at the same locations, and the results were coherent regardless the modelling choice. It is also worth noting that in the 8-story and the 12-story frames plastic hinges always formed in the external columns of the ground floor but not always in the internal columns, though these latter are

subjected to greater moments, because the effective strength of the external columns can be significantly reduced with respect to the nominal value due to the variation of axial load during lateral swinging of the building.

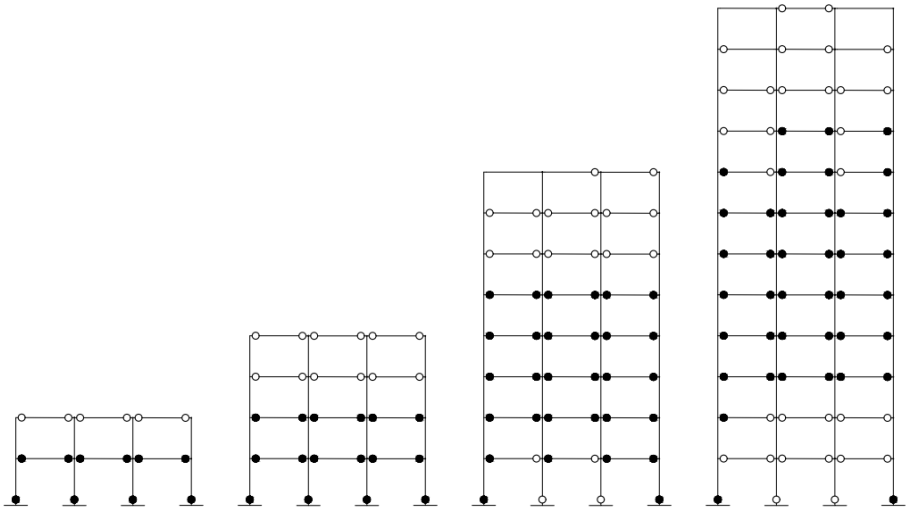

Figure 3: Locations of the plastic hinges triggered in the case-study frames

At the end of the time-history analyses, the response of the case-study structures has been evaluated considering engineering demand parameters such as inter-story drifts, absolute accelerations, and maximum forces and moments in the ground floor columns. During the post-processing of the analysis results relevant to each case-study frame, the maxima of each demand parameter have been identified for each time-history analysis (i.e. for each ground motion in Table 9); then, the mean value of these maxima has been computed for each plasticity formulation and evaluated. A detailed comparison among local-level response of the models is out of the scope of the present work.

Figure 4 to Figure 7 show the results obtained from the analyses performed considering the combination of the various plastic hinge lengths with a 50% reduction of the area moment of inertia ($I_{0.5I_g}$) for the elastic interior of beam and column members, compared to the results provided by the distributed plasticity formulation (FIBER). The comparison is made in terms of maximum inter-story drift ratio Δ_{max} and maximum Peak Floor Acceleration PFA_{max} evaluated over the whole structure, and maximum base shear V_{max} and base moment M_{max} in ground floor columns.

Regardless of the modeling approach, i.e. whether distributed or concentrated plasticity is implemented, and the adopted plastic hinge formulation, the 2-story and 4-story frames present the maximum inter-story drift ratio at the second floor, the 8-story frame at the third floor and the 12-story frame at the sixth floor; the maximum accelerations always occur at the last floor of each frame, while the most stressed elements across the frames are the internal columns at the ground floor, and for this reason, in the study the maximum base shear and the maximum base moment will always refer to these members.

Figure 4 shows the results for the maximum inter-story drift ratio Δ_{max}: the panel on the left compares the estimates provided by the various L_{pl} formulations, while the panel on the right shows the relative deviation (in %) of each estimate from the benchmark value provided from the distributed inelasticity model. For the 2-story, 4-story and 8-story frames the concentrated plasticity models underestimate the benchmark response (Figure 4a); more precisely, the deviation is on the order of -10% for CEN, FAR, P-P and P-F formulations, whichever the frame, while the ELM and the NTC models provide a better agreement for the 4-story and the 8-story frames, with deviations on the other of -5% (Figure 4b). The opposite behavior is noticed for the 12-story frame: CEN, FAR, P-P and P-F formulations are in good agreement with the benchmark, while ELM and NTC overestimate it by about 5%. Only for the 2-story building the drift is not significantly affected by the assumed plastic hinge model.

Also for the maximum base moment M_{max} (Figure 5) the concentrated plasticity models underestimate the results of the distributed plasticity representation, though providing values comparable to each other. Relative deviations from the benchmark are on the order of -5% for the 2-story and 4-story frames, but rise to -10% for medium-rise buildings.

A fair agreement between the concentrated and the distributed plasticity formulations is found when the maximum base shear force and the maximum Peak Floor Acceleration are examined, with deviations in general smaller than 5% (Figure 6 and Figure 7). Regarding PFA_{max}, with P-P, P-F, FAR and CEN formulations the relative deviation (Figure 6b) is positive for low-rise frames, and

negative for the 8-story and the 12-story frames, but always less than 3%; the ELM and NTC models show a very fair agreement with the benchmark for all the buildings but for the 12-story frame, for which the deviation is on the order of 7 – 8%.

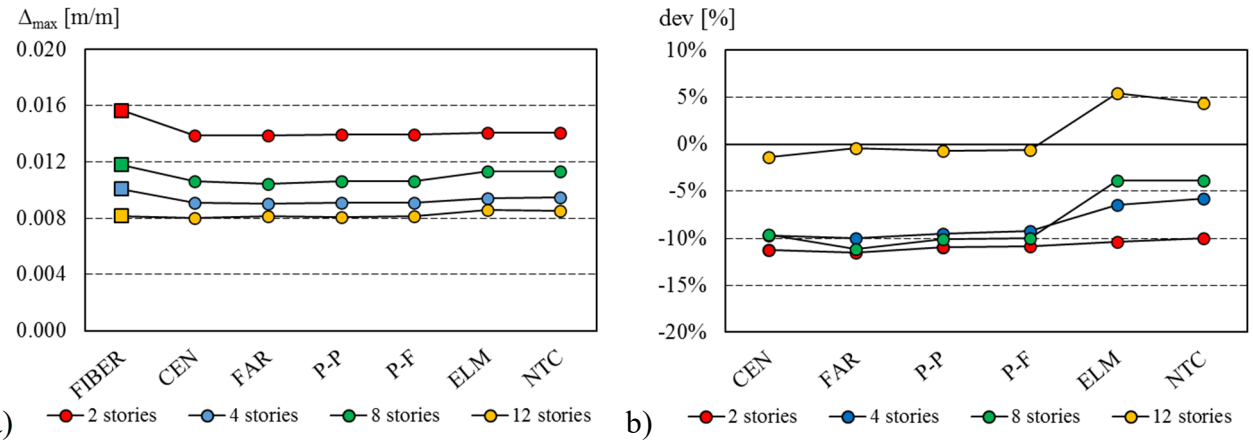

a) b)

Figure 4: Maximum inter-story drift ratio Δ_{max} (combination of L_{pl} with $I_{0.5I_g}$)

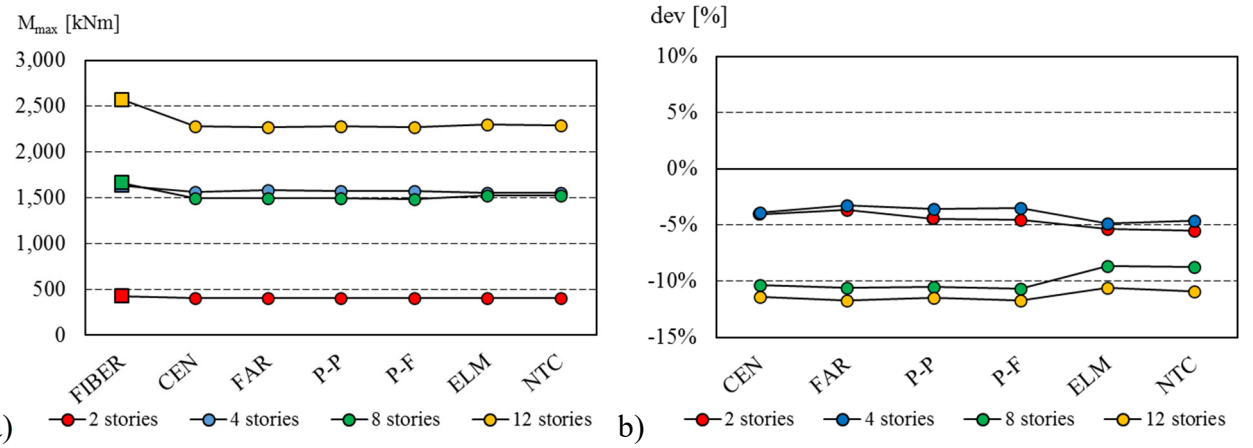

a) b)

Figure 5: Maximum base moment M_{max} (combination of L_{pl} with $I_{0.5I_g}$)

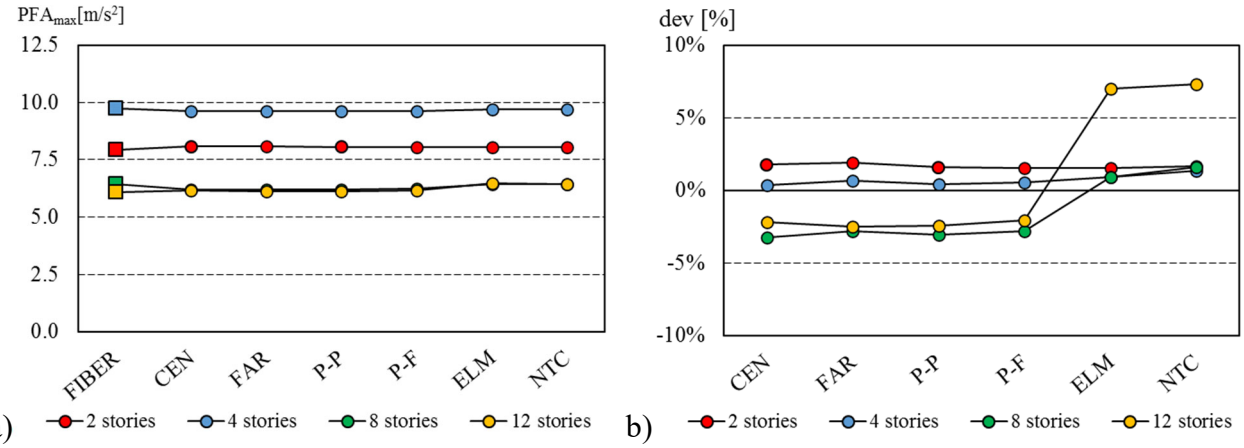

a) b)

Figure 6: Maximum Peak Floor Acceleration PFA_{max} (combination of L_{pl} with $I_{0.5I_g}$)

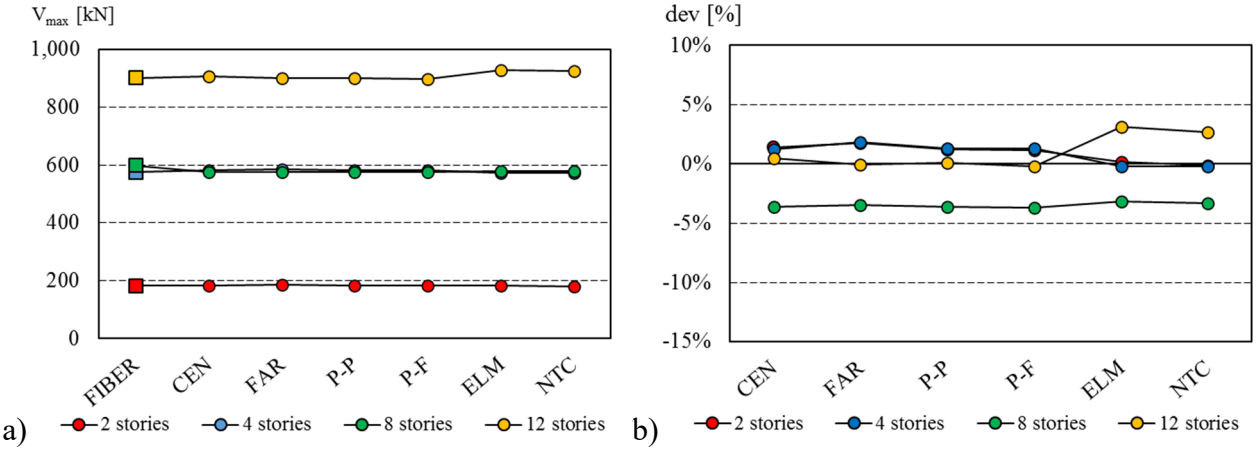

a) b)

Figure 7: Maximum base shear force V_{max} (combination of L_{pl} with $I_{0.5I_g}$)

Figure 8 to Figure 11 show the results obtained from the analyses performed combining the concentrated plasticity formulations with the effective area moment of inertia I_P according to Eq.(9).

In general, the lumped plasticity formulations keep underestimating the maximum inter-story drift ratio Δ_{max} (Figure 8) predicted in the distributed plasticity approach (with only few exceptions, e.g., the 12-story frame with ELM or NTC models), but the agreement is significantly improved in comparison to Figure 4 for the 4-story and the 8-story frames: for the first structure, the deviations from the distributed plasticity benchmark become negligible, and for the second one, the deviation is on the order of 4% for ELM and CEN formulations, and of 6-7% for the other models. In contrast, there is no apparent benefits when the 12-story frame is considered: for ELM and NTC models the

accord does not change, while for the others the deviation changes from a virtually zero value to about -5%. For the 2-story frame there is no substantial change with respect to Figure 4.

The maximum Peak Floor Acceleration PFA_{max} estimates (Figure 9) do not change significantly for the 2-story and the 4-story frames with respect to the results shown in Figure 6, while the agreement with the benchmark improves for the 8-story frame: notably, for these three frames the lumped plasticity formulations show a fair agreement with the distributed plasticity approach. For the 12-story frame the PFA_{max} is slightly overestimated by the plastic hinge formulations, with a deviation on the order of 5% for all models but for ELM and NTC models which have a deviation higher than 7%.

Also for the maximum base shear V_{max} (Figure 10), the results of the concentrated plasticity models are not significantly affected from the adopted expression for the effective area moment of inertia, and are comparable to those shown in Figure 7, confirming an acceptable agreement with the distributed plasticity approach (deviation less than 5%).

A remarkable improvement on the estimate of M_{max} is instead evident by comparing Figure 11 to Figure 5; the deviation between the lumped plasticity models and the benchmark is reduced to values below 10%, and for the 4-story frame, in some cases the deviation is even negligible. Anyway, the results confirm that the agreement is better for low-rise than for medium-rise frames, and the influence of the adopted plastic hinge formulation is generally low.

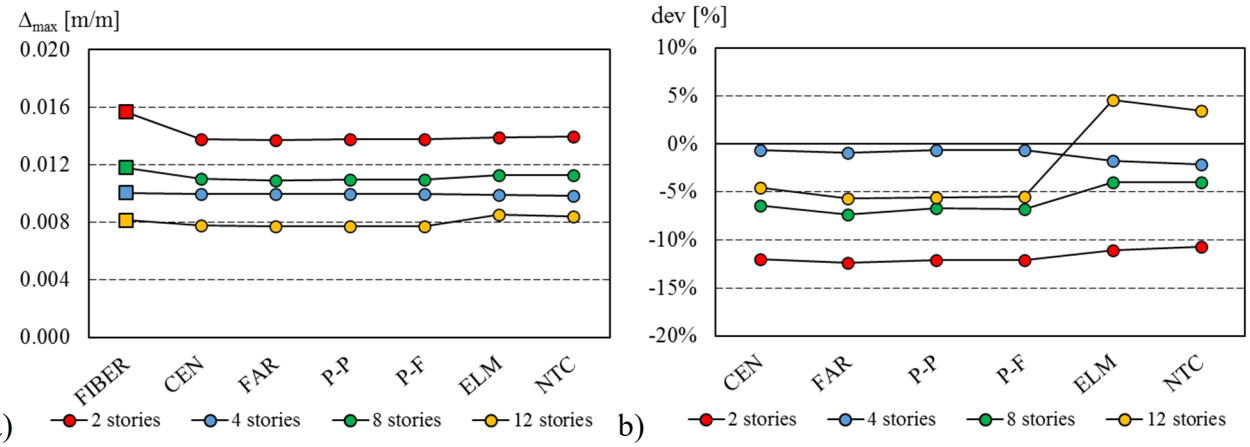

a) b)

Figure 8: Δ_{max} and % of deviation (combination of L_{pl} with I_P)

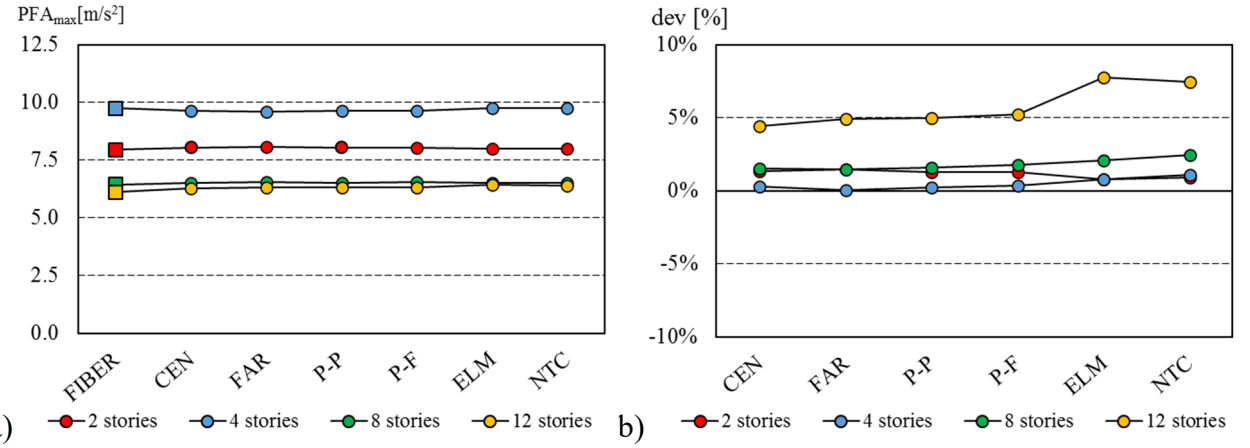

a) b)

Figure 9: PFA_{max} and % of deviation (combination of L_{pl} with I_P)

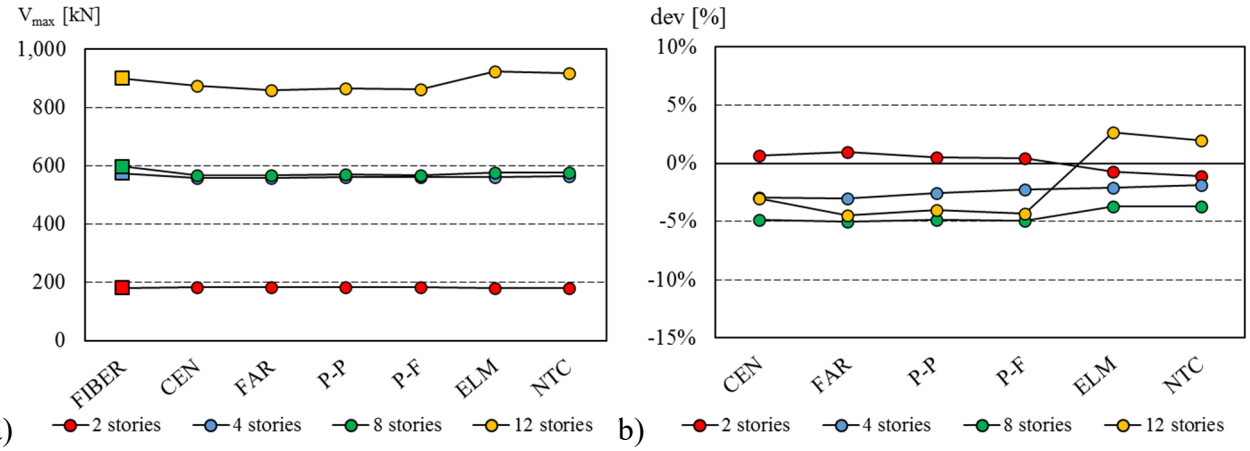

a) b)

Figure 10: V_{max} and % of deviation (combination of L_{pl} with I_P)

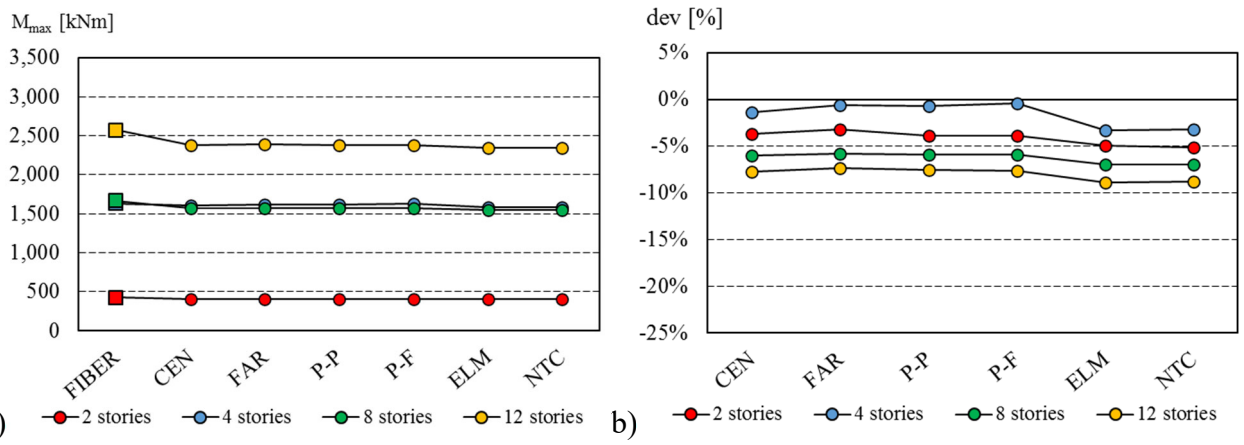

Figure 11: M_{max} and % of deviation (combination of L_{pl} with I_P)

Non-structural components, such as supply lines, plants and architectural elements, as well as technological content that may be present in the buildings, are sensitive to displacements and/or accelerations [69]; for this reason, a second comparison is made in terms of peak inter-story drift ratio Δ and peak floor acceleration PFA at each floor. The results shown in Figure 12(a) to Figure 19(a) pertain to FIBER, P-P, CEN and ELM formulations combined with the effective area moment of inertia $I_{0.5\mathrm{I_g}}$ according to Eq. (10), and those shown in Figure 12(b) to Figure 19(b) pertain to P-P, CEN and ELM formulations combined with I_P according to Eq.(9). For sake of brevity, the results associated to P-F, FAR and NTC models have been omitted because very close to the ones relevant to P-P and ELM, respectively.

As apparent in Figure 12 to Figure 15, the lumped plasticity models generally provide a stiffer behavior than the distributed plasticity approach, underestimating the inter-story drift at each floor. However it is noted that for the 12-story frame the ELM model overestimates, in particular at floors 6 and 7 where the largest drifts occur, the response calculated by the FIBER model, consistently with the results presented in Figure 4 and Figure 8.

In contrast, the predicted Peak Floor Acceleration is not substantially affected by the modelling choice (Figure 16 to Figure 19), even though for the 12-story frame the concentrated plasticity models predict

slightly higher accelerations at the top floor than the benchmark. These results are consistent with those shown in Figure 6 and Figure 9.

Analyzing more in detail the effects of the modelling choices, the estimates of drift ratio and peak floor acceleration of the 2-story frame (Figure 12 and Figure 16) seem to be affected neither by the choice of L_{pl} nor by the effective area moment of inertia. However, while the differences from the distributed plasticity model in terms of PFA are negligible, the drifts are significantly underestimated.

For the 4-story frame the agreement on drift estimates is significantly improved by combining L_{pl} with I_P, and the diagrams of the various models practically overlap (Figure 13b). For the 8-story and 12-story frames, the differences among the models are more evident, in particular, when I_{eq} is taken as $I_{o.5I_g}$: the ELM curve is the closest to the benchmark at each floor, while CEN and P-P plots, though in good agreement with each other, underestimate the FIBER values. The discrepancy between the lumped plasticity models and the benchmark are reduced when I_{eq} is assigned as I_P, Figure 14b and Figure 15b.

Little influence of the effective area moment of inertia is instead found on the estimate of floor acceleration. In general, the agreement on PFA is already very good among all models when $I_{0.5I_g}$ is assigned, and switching to I_P does not lead to any practical improvement. Actually, only for the 12-story building (Figure 19) a certain mismatch is observed between P-P and CEN models on one side, and FIBER and ELM models on the other side, but the difference, which concerns only the intermediate floors, is within 10%, and does not affect PFA_{max} which is attained at the top floor.

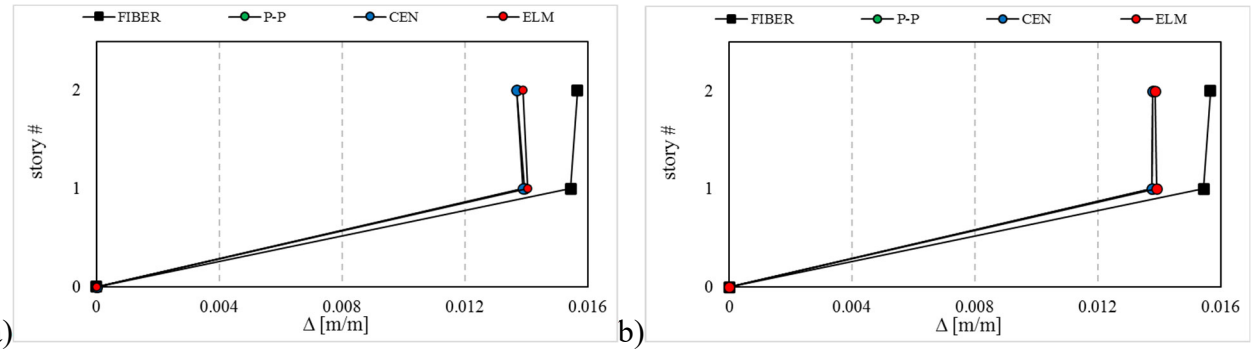

a) b)

Figure 12: Inter-story drift ratio Δ across the 2-story frame: a) a) $I_{0.5I_g}$; b) I_P

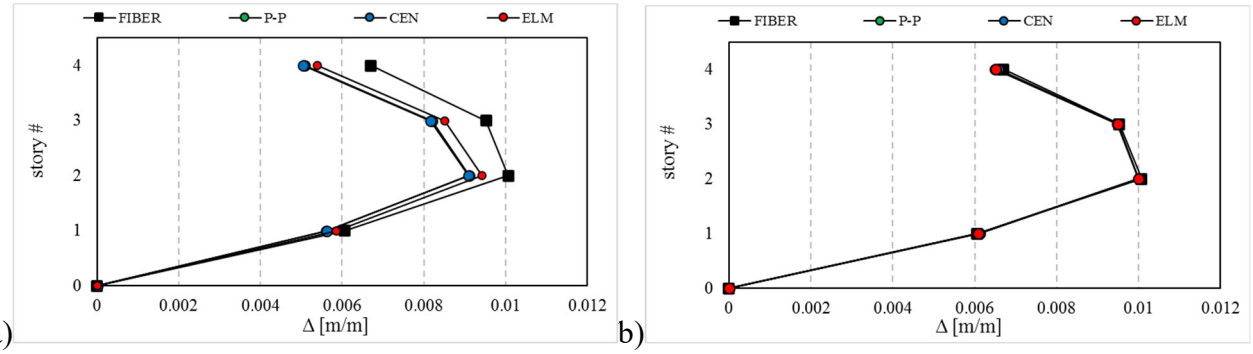

a) b)

Figure 13: Inter-story drift ratio Δ across the 4-story frame: a) $I_{0.5I_g}$; b) I_P

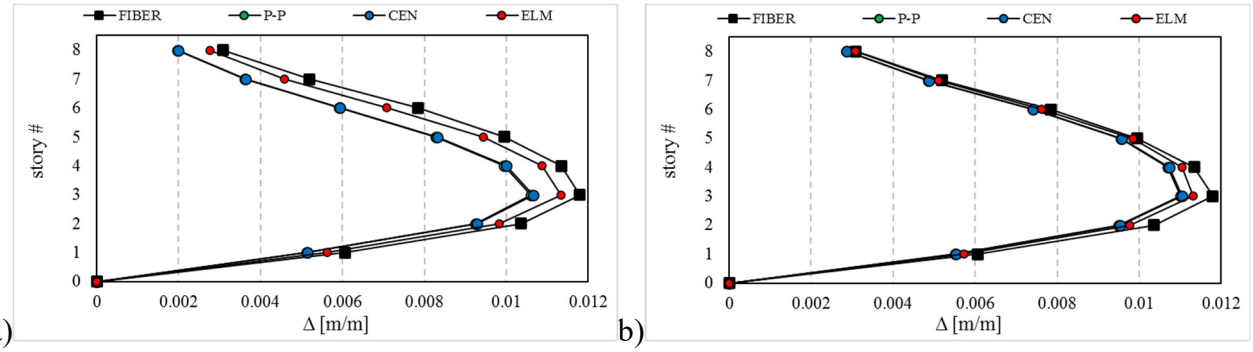

a) b)

Figure 14: Inter-story drift ratio Δ across the 8-story frame: a) $I_{0.5I_g}$; b) I_P

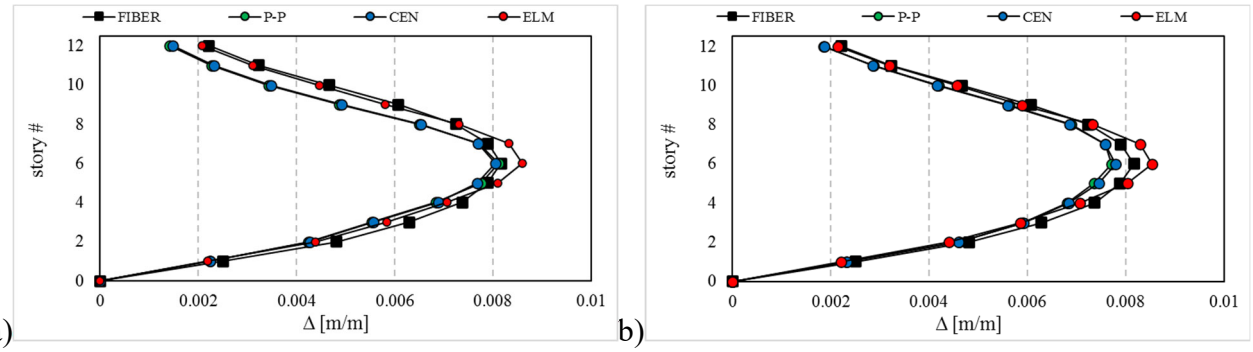

Figure 15: Inter-story drift ratio Δ across the 12-story frame: a) $I_{0.5\mathrm{I_g}}$; b) I_P

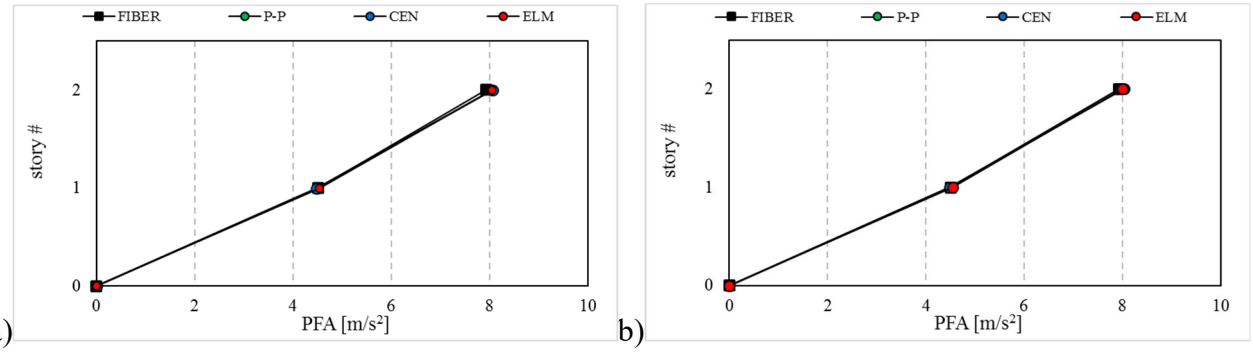

Figure 16: Peak Floor Acceleration PFA across the 2-story frame: a) $I_{0.5I_g}$; b) I_P

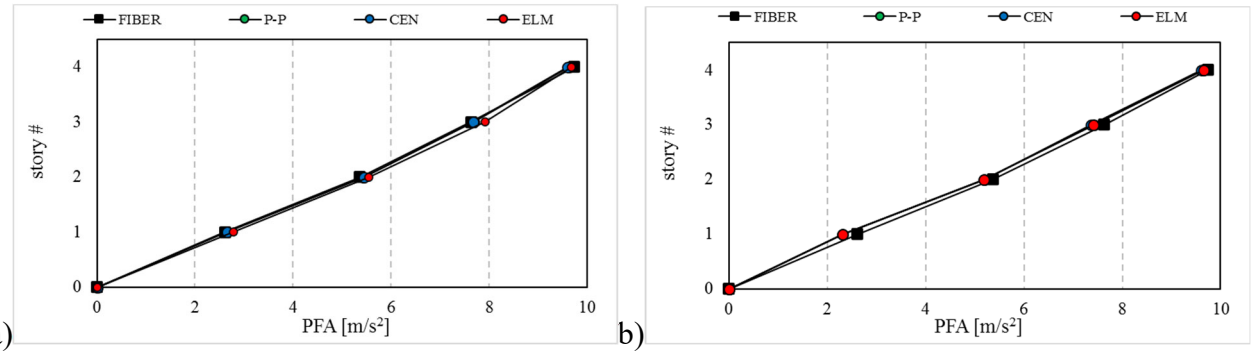

Figure 17: Peak Floor Acceleration PFA across the 4-story frame: a) $I_{0.5I_g}$; b) I_P

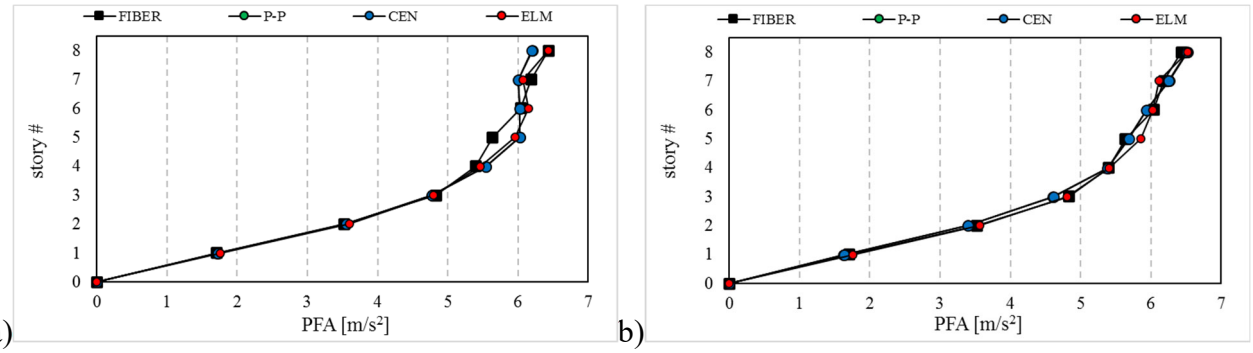

Figure 18: Peak Floor Acceleration PFA across the 8-story frame: a a) $I_{0.5I_g}$; b) I_P

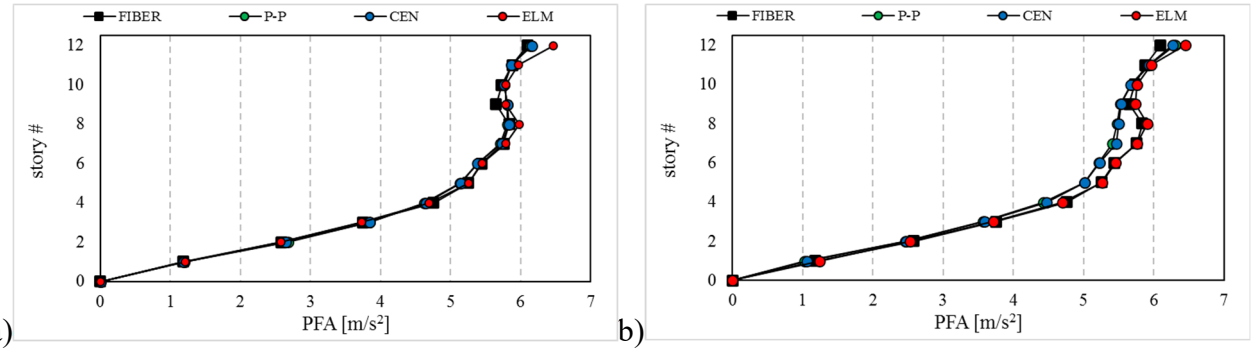

Figure 19: Peak Floor Acceleration PFA across the 12-story frame: a a) $I_{0.5I_g}$; b) I_P

5. Discussion

The engineering demand parameters that appear to be mainly affected by the modelling decisions are the inter-story drift ratio Δ and the maximum moment in the ground floor columns M_{max}, while the peak floor acceleration PFA and the maximum base shear V_{max} are less influenced. When a 50% reduction of the gross area moment of inertia $I_{0.5I_g}$ of the cracked concrete section is assigned to every beam and column member, plastic hinge lengths according to the ELM and NTC formulations provide estimates more in agreement with the distributed plasticity approach (Figure 4, Figure 12 to Figure 15). This especially occurs when the medium-rise (8-story and 12-story) frames are analyzed. In contrast, the results of the 2-story frame are practically unaffected by the modelling choices, and the inter-story drifts of the benchmark model are considerably underestimated regardless of the assumed plastic hinge length or the effective area moment of inertia, whereas the agreement on the internal forces in the most stressed columns at the ground floor is very fair.

The performances of the various formulations can be explained by considering the extension of the plastic hinge region associated to each model, as shown in Figure 20. P-P and P-F formulations provide very close values of L_{pl}, both for column members (L_{pl} from 0.30 to 0.33 m) and for beam members (L_{pl} from 0.35 to 0.38 m), whichever the analyzed frame, and indeed these two models yield similar results, as shown in Figure 12 to Figure 19. The two models account, in the expression of L_{pl}, for the contributions of the shear span z and of the longitudinal reinforcement (Table 1): indeed P-F assumes a 50% higher contribution of z than P-P, but this is counterbalanced by a lower influence of the reinforcement contribution $d_b f_y$. The FAR formulation anticipates shorter plastic hinge lengths than the previous two models, especially for the 2-story and the 4-story frames, but the difference disappears in taller structures. It is worth recalling that in the theory underlying the FAR formulation the dependence upon the reinforcement is not explicit in the formulation of L_{pl} but it is included in the expressions of the rotations at yielding and failure (Table 8).

The ELM formulation accounts, as an additional contribution, for the length of the shear spread, which is more important in beam than in column members. The predicted plastic hinge length is the largest among all the examined models, and ranges from 0.45 to 0.75 m for columns and from 0.50 to about 0.8 m for beams (Figure 20) depending on the considered frame.

The expressions of L_{pl} provided by the European and the Italian codes depend on the shear span, the section depth and the longitudinal reinforcement, but assign different weights to each contribution (Eq.(2) and Eq.(3)). Therefore, the plastic hinge lengths calculated according to NTC are about two times greater than their CEN counterparts, and close to ELM's. In this regard it is worth noting that in the 8-story and 12-story frames the plastic hinge lengths calculated according to NTC and ELM formulations stretch to about 1/6 of the total length of each structural member; in contrast, plastic hinge lengths according to P-P, P-F and FAR formulations are on the order of 10% of the member length for columns, and 8% for beams; intermediate values are provided by the CEN formulation. But for P-P and P-F models, the length of plastic hinge region increases with the number of stories, which explains the poor agreement with the distributed plasticity model in terms of inter-story drift observed in the 2-story frame.

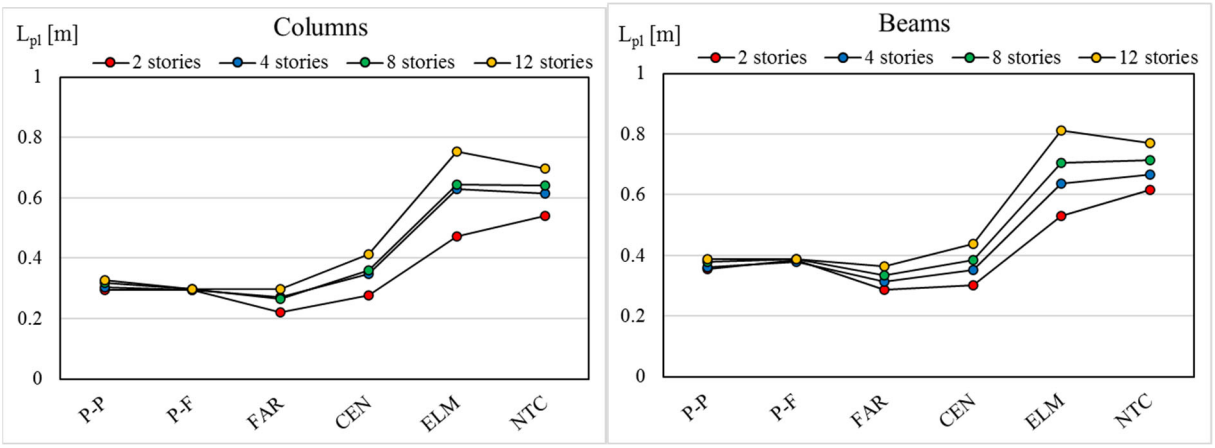

Figure 20: Plastic hinge length L_{pl} for column and beam members

Disregarding the ELM and NTC models, for which the benefit is indeed negligible, the estimates of demand parameters provided by the concentrated plasticity formulations show an improved

agreement with the distributed plasticity benchmark when the reduction of the gross area moment of inertia is assigned according to Eq. (9), i.e. $I_{eq} = I_P$. This formula indeed, which accounts for the contribution of the axial load, differentiates between column and beam members, and among columns at different floors. The ranges of the coefficients of reduction of I_P with respect to the area moment of inertia of the gross cross-section I_g calculated by Eq. (9) for the examined case-study frames are reported in Table 10. Beams, characterized by negligible axial force, have coefficients of reduction considerably lower than columns subjected to high axial load, which has a beneficial effect in increasing the cross-section nominal flexural strength. It is worth noting that the reduction coefficients shown in Table 10 are comparable to the ones prescribed in the New Zealander norm [31].

Member	***2 stories***	***4 stories***	***8 stories***	***12 stories***
Beam	0.37	$0.25 - 0.3$	$0.24 - 0.28$	$0.22 - 0.34$
Column, internal	$0.57 - 0.6$	$0.53 - 0.46$	$0.56 - 0.58$	$0.52 - 0.58$
Column, perimetral	$0.56 - 0.57$	$0.53 - 0.54$	$0.55 - 0.59$	$0.54 - 0.59$

Table 10: Reduction coefficients of the gross area moment of inertia of the case-study frames according to Eq.(9)

As highlighted in Figure 8, for the 4-story, 8-story and 12-story frames the concentrated plasticity models combined with the reduced area moment of inertia I_P yield estimates of Δ_{max} which deviate less than 10% from the benchmark; these results are also confirmed from the plots reported in Figure 13 to Figure 15 which show that the global deformation of the distributed plasticity model is well captured, especially for the 4-story frame. Good agreement is obtained also in terms of PFA, PFA_{max} and V_{max} (Figure 9, Figure 10, and Figure 16 to Figure 19) with scatter less than 5%, even if these response parameters are less affected by the choice on I_{eq}. Also for M_{max} assigning $I_{eq} = I_P$ leads to an improved agreement for P-P, P-F, FAR and CEN models (Figure 11). Generally speaking, the

adoption of the area moment of inertia I_P dependent upon the axial load benefits more those lumped plasticity models which are characterized by a "short" plastic hinge length than those anticipating a "long" L_{pl} (e.g., ELM and NTC models), which indeed stretches across a significant part of the total length of the structural member and consequently is likely to envelop the actual cracked region.

The effective area moment of inertia I_P does not carry any substantial improvement in the analyses of the 2-story frame. Therefore, regarding the accuracy of the results, the lumped plasticity approach does not seem a viable alternative to distributed plasticity modelling for very short-rise buildings.

The results presented in this study highlight that for non-linear analyses of framed RC buildings adopting a lumped plasticity formulation in accordance with Eurocode 8 [24] or with the Italian Building Code [25], the agreement with the results of a full distributed plasticity formulation can be substantially improved, in terms of inter-story drifts and maximum base moments, when the effective area moment of inertia I_{eq} of the elastic region of each member is assigned according to the formula given in Eq.(9) accounting for the effect of the axial load, rather than according to the formula $I_{eq} = 0.5I_g$ provided in the Codes themselves. This suggests that a more realistic approach is to differentiate the value of I_{eq} between either beam or column members, as well as among columns subjected to different levels of axial load, in line with other norms [31] [32].

6. Conclusions

The study investigates the performance of concentrated plasticity models used to represent the non-linear response of RC frames with flexural behavior in the context of time history analyses. The models were formulated in the OpenSees framework using the *forceBeamColumn* element object [7] coded in the software libraries, considering different modelling choices pertaining to the length of the plastic hinge region L_{pl} and the effective area moment of inertia I_{eq} of the cracked concrete section. Four reinforced concrete frames with 2, 4, 8 and 12 stories were taken as case-study structures. The frames were designed in compliance with the current code recommendations and according with the principles of the capacity design, avoiding brittle collapse; other failure mechanisms, such as bond slip or low-cycle fatigue, were not considered as well. Non-linear dynamic analyses were performed, and the response of the frames evaluated under a set of seven spectrum-compatible earthquakes according to the Italian Building Code [37]. Only plastic hinge formulations valid for cyclic loading and applicable to both column and beam members were taken into account.

The main outcomes of the research are summarized in the next points:

(1) depending on the modelling decision, the plastic hinge length L_{pl} varied between 10% and 20% of the member length for columns, and between 8% and 16% of the member length for beams, and, in the examined frames, was also affected from the height of the building, with greater lengths anticipated for taller structures; these differences were reflected in the analyses, with closer results provided by the models yielding comparable values of L_{pl};

(2) all the concentrated plasticity models were able to capture the global mechanical response of the case-study buildings predicted according to a distributed plasticity formulation, and to identify the locations where plastic hinges were triggered;

(3) regardless the choice of the plastic hinge length L_{pl} and the effective area moment of inertia I_{eq} of cracked concrete sections, estimates of absolute acceleration and maximum base shear provided by the concentrated plasticity models were in acceptable agreement with the distributed plasticity

benchmark; in contrast, lumped plasticity models tended to underestimate the inter-story drift ratio and the maximum base moment in all frames, with the only exceptions of the 12-story frame , where the drifts were overestimated by the ELM and NTC models; better agreement on the maximum base moment was consistently achieved in low-rise than in medium-rise buildings;

(4) regarding the modelling choice used to account for the reduced flexural strength of the cracked concrete section, a closer agreement with the results provided from the distributed plasticity approach was achieved by assigning an area moment of inertia dependent upon the axial load (Eq.(9) in the paper), rather than a fixed 50% reduction of gross area moment of inertia as recommended in the European [50] and the Italian [37] codes. The improvement was more evident for lumped plasticity formulations anticipating a "short" plastic hinge length than a "long" L_{pl}; in the latter case, the assigned region, where plastic deformation is allowed to occur, indeed extends over a significant part of the total length of the structural member and consequently is likely to envelop the actual cracked region;

The results of the study therefore suggest that, but for very low-rise frames like, e.g., the 2-story frame examined in the study, a better agreement with the results of distributed plasticity analyses, especially in terms of maximum inter-story drift ratio and maximum base moment, can be achieved by adopting different values of I_{eq} for either beams or columns, as well as for columns subjected to different levels of axial load, in line with the provisions of other norms [31] [32].

It should be noted that these conclusions might only apply to buildings exhibiting a strong-column/weak-beam behavior in line with the capacity design. The results were obtained examining four frames, from two to twelve stories in height, characterized by a regular distribution in plan and elevation, and considering only a set of seven ground motions. Though the number of ground acceleration histories is in accordance with the prescriptions of the Italian Building Code [37], bias-related issues due to the low number of ground motions may be a concern. In a future development the investigation will be extended to buildings with irregular plant and will consider a larger number of ground motions, representing different site characteristics and comprising both near-fault and far-

field events, in order to confirm the validity of the present conclusions over a large variety of practical conditions. Nevertheless, despite these current limitations, the Authors believe that the study has some merit in providing, for the first time, a comprehensive comparison between the effects of the modelling decisions in the formulation of concentrated plasticity models for non-linear dynamic analyses of ductile RC frames.

Symbols

a_v zero-one coefficient related to the cracking phenomena due to shear or flexure

A_g gross area of concrete section

A_s area of tension reinforcement

A_{st} area of transverse reinforcement

b strain-hardening ratio

B section width of the structural element

B_p section width of the pillars

CR_1 curvature degradation parameter

CR_2 curvature degradation parameter

d section depth of tension reinforcement

d' section depth of compression reinforcement

d_b diameter of longitudinal reinforcement

d_{st} diameter of transverse reinforcement

E_c modulus of elasticity of concrete

E_s modulus of elasticity of steel

f_c compressive strength of concrete

f_{cc} compressive strength of confined concrete

f_{cover} compressive strength of the concrete cover

f_{ct} tensile strength of the concrete section

f_l' effective lateral confining stress on concrete

f_y yielding stress of longitudinal reinforcement

f_{yw} yielding stress of transverse reinforcement

f_u ultimate tensile strength of reinforcement

G_1 permanent structural loads

G_2 non-permanent structural loads

h overall depth of beam or column

h_c section height of the confined core

$I_{0.5I_g}$ effective area moment of inertia evaluated according to Eq.(10)

I_{cr} area moment of inertia of the cracked section

I_{eq} effective area moment of inertia

I_g gross area moment of inertia

I_P effective area moment of inertia evaluated according to Eq.(9)k_1 = 0.7 for mild steel, 0.9 for cold worked steel [8]

$k_2 = 1 + 0.5P/P_0$ used in [8]

$k_3 = 0.9 - \left(\frac{0.3}{23.5}\right)(f_c - 11.7)$ (f_c in MPa) [8]

L_{pl} plastic hinge length

l_s length of shear spread

M_b bending moment acting on the section

M_{cr} bending moment at the first cracking

M_{max} maximum base moment (in the most stressed column at the ground floor)

M_N nominal flexural moment

M_y yield flexural moment

M_w magnitude

N axial load under gravity actions alone

P applied axial force [18] [20] [21]

$P_0 = 0.85f_c(A_g - A_s) + f_y A_s$ nominal axial load capacity as per ACI 318 [23] used in references [18], [20], [21]

PFA peak floor acceleration

PFA_{max} maximum peak floor acceleration across the frame

PGA peak ground acceleration

q tension reinforcement index $\left(= \frac{A_s}{bd} \cdot \frac{f_y}{f_c}\right)$ [9]

Q live loads

q' compressive reinforcement index $\left(= \frac{A_s'}{bd} \cdot \frac{f_y}{f_c}\right)$ [9]

q_b balanced tension reinforcement index $\left(= \frac{A_b}{bd} \cdot \frac{f_y}{f_c}\right)$ [9]

R_{ep} epicentral distance

R_0 initial value of the curvature parameter

s spacing of the transverse reinforcement

SF scale factor

t duration of the earthquake

T_1 period of the first vibration mode of the frames

T_2 period of the second vibration mode of the frames

V_{max} maximum base shear (in the most stressed columns at the ground floor)

z distance from critical section of maximum curvature and the element point of contraflexure

α coefficient depending on the type of structural element (0.108 for columns, 0.133 for beams, 0.152 for rectangular walls) [16]

α_c confinement effectiveness factor

γ_{el} = 1.5 for primary seismic elements, = 1 for secondary seismic elements

Δ inter-story drift ratio

Δ_{max} maximum inter-story drift ratio across the frame

δ ultimate top displacement of an RC cantilever column

ε_c floating point value defining concrete strain at maximum strength

ε_{c2} strain at which f_{cc} is attained in accordance with the model of Eurocode 2 [46]

ε_{cc} strain at which f_{cc} is attained in accordance with the model of Eurocode 8 [24]

ε_{cu} floating point value defining concrete strain at crushing strength

ε_{sm} steel strain at maximum tensile stress

ε_{su} ultimate elongation of steel

ε_t tensile strain of the concrete section

ε_y yield strain of the longitudinal reinforcement

ζ level arm equal to $d - d'$ in rectangular sections

θ_y chord rotation at yielding

$\theta_{y,slip}$ yielding rotation due to slippage of longitudinal bars from the anchorage zone

$\theta_{u,slip}$ ultimate rotation due to slippage of longitudinal bars from the anchorage zone

$\nu = \frac{N}{A_g f_c}$ axial load ratio [16]

φ_y yield curvature

φ_u ultimate curvature at failure

ρ_c ratio of longitudinal reinforcement in compression

ρ_d ratio of diagonal reinforcement (if present)

ρ_l total longitudinal reinforcement ratio

ρ_s volumetric ratio of confining steel

ρ_{sx} ratio of transverse steel parallel to the direction x of loading

ρ_t ratio of longitudinal reinforcement in tension

ω mechanical ratio of the tension longitudinal reinforcement

ω' mechanical ratio of the compression longitudinal reinforcement

Acknowledgments

The work was developed during the research fellowship of Eleonora Bruschi at the University of Washington sponsored by the Ermenegildo Zegna Founder's Scholarship (2018).

References

[1] McKenna F, Fenves GI, Scott MH. Open System for Earthquake Engineering Simulation, PEER Report, Berkeley, CA; 2000.

[2] Dassault Systemes Simulia Corp. Abaqus/CAE user's guide, Providence, RI, USA; 2017.

[3] CSPFEA. Midas Gen FX Manual, CSPFEA Engineering solutions. http://www.cspfea.net/portfolio_page/midas-gen-fx/; 2018.

[4] Brunetta M, Bandini L, De Lorenzi M. SAP2000, analisi lineare/nonlineare integrata con verifiche per strutture tridimensionali. CSI Computer and Structures Inc; 2006.

[5] Calabrese A, Almeida JP, Pinho R. Numerical Issues in Distributed Inelasticity Modeling of RC Frame Elements for Seismic Analysis, Journal of Earthquake Engineering 2010;14: S1:38-68; https://doi.org/10.1080/13632469.2010.495681.

[6] Wu RY, Pantelides CP. Concentrated and distributed plasticity models for seismic repair of damaged RC bridge columns. Journal of Composites for Construction 2018, 10.1061/(ASCE)CC.1943-5614.0000879, 04018044.

[7] Scott MH, Fenves GL. Plastic Hinge Integration Methods for Force-Based Beam-Column Elements, Journal of Structural Engineering 2006; 132(2):244-252; https://doi.org/10.1061/(ASCE)0733-9445(2006)132:2(244).

[8] Baker ALL. Ultimate Load Theory Applied to the Design of Reinforced and Prestressed Concrete Frames, Concrete Publications Ltd, London, UK; 1956, 91 pp.

[9] Mattock AH. Rotational Capacity of Hinging Regions in Reinforced Concrete Beams, Flexural Mechanics of Reinforced Concrete, SP-12, American Concrete Institute: Farmington Hills, MI; 1964, p. 143-181.

[10] Sawyer HA. Design of concrete frames for two failure stages. In Proceedings of international symposium on the flexural mechanics of reinforced concrete, Miami; 1964, ACI SP-12:405-431.

[11] Corley WG. Rotational Capacity of Reinforced Concrete Beams, Journal of the Structural Division, ASCE 1966;92: ST5:121-146.

[12] Mattock AH. Discussion of Rotational Capacity of Hinging Regions in Reinforced Concrete Beams, Journal of the Structural Division, ASCE 1967;93: ST2:519-522.

[13] Priestley MJN, Park R. Strength and Ductility of Concrete Bridge Columns Under Seismic Loading, ACI Structural Journal 1987;84(1):61-76.

[14] Paulay T, Priestley MJN. Seismic Design of Reinforced Concrete and Masonry Buildings, John Wiley and Sons, New York; 1992, 767 pp.

[15] Panagiotakos TB, Fardis MN. Deformation of reinforced concrete members at yielding and ultimate, ACI Structural Journal 2001;98(2):135-148.

[16] Fardis MN. LESSLOSS – Risk mitigation for earthquakes and landslides, Guidelines for displacement – based design of buildings and bridges, Report n. 5/2007, IUSS Press, Pavia, Italy; 2007.

[17] Priestley MJN, Calvi GM, Kowalsky MJ. Displacement-based seismic design of structures. IUSS Press, Pavia 2007.

[18] Bae S, Bayrak O. Plastic hinge length of reinforced concrete columns, ACI Structural Journal 2008;105(3):290-300; retrieved from https://search.proquest.com/docview/198338935?accountid=28385.

[19] Elmenshawi A, Brown T, El-Metwally S. Plastic Hinge Length Considering Shear Reversal in Reinforced Concrete Elements, Journal of Earthquake Engineering 2012;16(2):188-210; https://doi.org/10.1080/13632469.2011.597485.

[20] Mortezaei A, Ronagh HR. Plastic Hinge Length of Reinforced Concrete Columns Subjected to Both Far-Fault and near-Fault Ground Motions Having Forward Directivity, Structural Design of Tall and Special Buildings 2013;22(12):903-926; https://doi.org/10.1002/tal.729.

[21] Ning CL, Bing L. Probabilistic Approach for Estimating Plastic Hinge Length of Reinforced Concrete Columns, Journal of Structural Engineering 2016;142(3): Article number 04015164; https://doi.org/10.1061/(ASCE)ST.1943-541X.0001436.

[22] FEMA (Federal Emergency Management Agency). FEMA 356. Prestandard and commentary for the seismic rehabilitation of buildings, Applied Technology Council for the Federal Emergency Management Agency, Washington, DC, 2000.

[23] ACI Committee 318. Building Code Requirements for Structural Concrete (ACI 318-19) and Commentary (ACI 318R-19), American Concrete Institute, Farmington Hills, MI, USA, 2019.

[24] CEN (European Committee for Standardization). Design of structures for earthquake resistance - Part 3: Assessment and retrofitting of buildings. EN 1998–3 Eurocode 8; 2005.

[25] CSLLPP (Consiglio Superiore dei Lavori Pubblici). Circolare 21 gennaio 2019, n. 7 C.S.LL.PP. Istruzioni per l'applicazione dell'«Aggiornamento delle "Norme tecniche per le costruzioni"» di cui al decreto ministeriale 17 gennaio 2018, Roma; 2019, in Italian.

[26] Teruna DR, Wijaya H. Seismic responses comparison of RC building in consideration of plastic hinge models and properties, IOP Conference Series: Material Science and Engineering 2018;383: Article number 012025; https://doi.org/10.1088/1757-899X/383/1/012025.

[27] Lima C, Angiolilli M, Barbagallo F, Belletti B, Bergami AV, Camata G, Cantagallo C, Di Domenica M, Fiorentino G, Ghersi A, Gregori A, Lavorato D, Luciano R, Marino EM, Martinelli E, Nuti C, Ricci P, Rosati L, Ruggieri S, Sessa S, Spacone E, Terrenzi M, Uva G, Vecchi F, Verderame GM. Nonlinear Modeling Approaches for Existing Reinforced Concrete Buildings: The Case Study of De Gasperi-Battaglia School Building in Norcia, Lecture Notes in Civil Engineering 2020;42:82-95; https://doi.org/10.1007/978-3-030-23748-6_7.

[28] Inel M., Ozmen HB. Effects of Plastic Hinge Properties in Nonlinear Analysis of Reinforced Concrete Buildings, Engineering Structures 2006;28(11):1494-1502; https://doi.org/10.1016/j.engstruct.2006.01.017.

[29] Lopez AL, Tomas A, Olivares, G. Influence of adjusted models of plastic hinges in nonlinear behavior of reinforced concrete buildings, Engineering Structures 2016;124:245-57; https://doi.org/10.1016/j.engstruct.2016.06.021.

[30] Petrini L, Maggi C, Priestley MJN, Calvi GM. Experimental Verification of Viscous Damping Modeling for Inelastic Time History Analyzes, Journal of Earthquake Engineering 2008, 12:S1, 125-145, DOI: 10.1080/13632460801925822.

[31] NZS (Standards Council of New Zealand). Concrete buildings. Part C – The design of concrete structures. NZS 2017.

[32] KANEPE, Hellenic Code of Retrofitting of Reinforced Concrete Buildings. Organization of Seismic Design & Protection (OASP). Gov. Gaz. 2984/B/30-8-2017. Hellenic Ministry of Infrastructure, Transport and Network, 2012. (in Greek).

[33] Lemes IJM, Barros RC, Silveira RAM, Silva ARD, Rocha PAS. Numerical analysis of RC plane structures: a concentrated nonlinear effect approach, Latin American Journal of Solids and Structures 2018:15(2) Article number e20; https://doi.org/10.1590/1679-78254681.

[34] Spacone E, Filippou F, Taucer F. Fibre beam-column model for non-linear analysis of r/c frames: part I. formulation, Earthquake Engineering and Structural Dynamics 1996a, 25, 711–726; doi: 10.1002/(SICI)1096-9845(199607)25:7<711:AID-EQE576>3.0.CO;2-9.

[35] Spacone E, Filippou F, Taucer F. Fibre beam-column model for non-linear analysis of r/c frames: part II. Applications, Earthquake Engineering and Structural Dynamics 1996b, 25, 727–742; doi: 10.1002/(SICI)1096-9845(199607)25:7<727:AID-EQE577>3.0.CO;2-O.

[36] Terrenzi M, Spacone E, Camata G. Comparison Between Phenomenological and Fiber-Section Non-linear Models, Frontiers in Built Environment 2020, 6:38; doi: 10.3389/fbuil.2020.00038.

[37] CSLLPP (Consiglio Superiore dei Lavori Pubblici). D.M. 17 gennaio 2018 in materia di "norme tecniche per le costruzioni". Gazzetta ufficiale n.42 del 20 febbraio 2018, Supplemento ordinario n.8, Ministero delle Infrastrutture e dei trasporti, Roma; 2018, in Italian.

[38] Pereira N, Romao X. Damage localization length in RC frame components: Mechanical analysis and experimental observations, Engineering Structures 221 (2020) 111026; https://doi.org/10.1016/j.engstruct.2020.111026.

[39] Elmenshawi A, Brown T. Deformation capacity of ultra-high strength concrete flexural elements subjected to inelastic load reversals, The Structural Design of Tall and Special Buildings 2010; https://doi.org/10.1002/tal.633.

[40] Park R, Paulay T. Reinforced Concrete Structures, John Wiley and Sons, New York, 1975, 769 pp.

[41] Verderame G, Ricci P, Manfredi G, Cosenza E. Ultimate Chord Rotation of RC Columns with Smooth Bars: Some Considerations about EC8 Prescriptions, Bulletin of Earthquake Engineering 2010;8(6):1351-1373; https://doi.org/10.1007/s10518-010-9190-x.

[42] Zhao X, Wu YF, Leung AYt, Lam HF. Plastic Hinge Length in Reinforced Concrete Flexural Members, Procedia Engineering 2011;14:1266-1274; https://doi.org/10.1016/j.proeng.2011.07.159.

[43] Yuan F, Yu-Fei W. Effect of Load Cycling on Plastic Hinge Length in RC Columns, Engineering Structures 2017;147:90-102; https://doi.org/10.1016/j.engstruct.2017.05.046.

[44] Ameli MJ, Pantelides CP. Seismic analysis of precast concrete bridge columns connected with grouted splice sleeve connectors, Journal of Structural Engineering 2017, ASCE, 10.1061/(ASCE)ST.1943-541X.0001678, 04016176.

[45] CEN (European Committee for Standardization). Design of structures for earthquake resistance – Part 2: Bridges. EN 1998–2 Eurocode 8; 2005.

[46] CEN (European Committee for Standardization). Design of concrete structures - Part 1-1: General rules and rules for buildings. EN 1992-1-1 Eurocode 2; 2005.

[47] Mander JB, Priestley MJN, Park R. Theoretical stress-strain model for confined concrete, Journal of Structural Engineering ASCE 1988; 114(8), 1804-1825.

[48] Branson DE, Metz GA. Instantaneous and time-dependent deflections of simple and continuous reinforced concrete beams, Auburn: Department of Civil Engineering and Auburn Research Foundation, Auburn University; 1963.

[49] Priestley, MJN. Brief Comments on Elastic Flexibility of Reinforced Concrete Frames and Significance to Seismic Design, Bulletin NZ National Society for Earthquake Engineering 1998;31(4):246-259.

[50] CEN (European Committee for Standardization). Design of structures for earthquake resistance - Part 1: General rules, seismic actions and rules for building. EN 1998–1 Eurocode 8; 2005.

[51] Pettinga JD, Priestley MJN. Dynamic behavior of reinforced concrete frames designed with direct displacement – based design, Journal of Earthquake Engineering 2005;9:309-330.

[52] Barbagallo F, Bosco M, Marino E, Rossi P. On the fibre modelling of beams in RC framed buildings with rigid diaphragm, Bulletin of Earthquake Engineering 2020;18:189-210; https://doi.org/10.1007/s10518-019-00723-z.

[53] Menegotto M, Pinto PE. Method of analysis for cyclically loaded RC plane frames including changes in geometry and non-elastic behaviour of elements under combined normal force and bending, IABSE: Symposium on resistance and ultimate deformability of structures acted on by well defined repeated loads 1973 – Final Report.

[54] Filippou FC, Popov EP, Bertero VV. Effects of Bond Deterioration on Hysteretic Behavior of Reinforced Concrete Joints, Report EERC 83-19 (1983), Earthquake Engineering Research Center, University of California, Berkeley.

[55] OpenSeesWiki, online manual. Available online at: https://opensees.berkeley.edu/wiki/index.php/Main_Page [last access: April 2021].

[56] Popovics S. A numerical approach to the complete stress-strain curve of concrete, Cement and Concrete Research 1973; 3(5): 583-599.

[57] Almeida JP, Tarquini D, Beyer K. Modelling approaches for inelastic behaviour of RC walls: multi-level assessment and dependability of results. Archives of Computational Methods in Engineering 23, no. 1 (2016): 69-100; DOI: 10.1007/s11831-014-9131-y.

[58] Mpampatsikos V, Nascimbene R, Petrini L. A critical review of the R.C. frame existing building assessment procedure according to Eurocode 8 and Italian Seismic Code. Journal of Earthquake Engineering 2008; 12(S1), 52-82; https://doi.org/10.1080/13632460801925020 .

[59] Wijesundara KK, Bolognin D, Nascimbene R, Calvi GM. Review of design parameters of concentrically braced frames with RHS shape braces. Journal of Earthquake Engineering 2009; 13(S1), 109 – 131; https://doi.org/10.1080/13632460902813331.

[60] Wijesundara KK, Rassati GA, Nascimbene R, Bolognini D. Seismic performance of brace-beam-column connections in concentrically braced frames. Structures Congress 2010; 930-942.

[61] Fagà E, Ceresa P, Nascimbene R, Moratti M, Pavese A. Modelling curved surface sliding bearings with bilinear constitutive law: effects on the response of seismically isolated buildings. Materials and Structures 2016; 49: 2179 – 2196, DOI 10.1617/s11527-015-0642-2.

[62] Priestley MNJ, Grant DN. Viscous damping in seismic design and analysis, Journal of Earthquake Engineering 2005; 9:sup2, 229-255, DOI: 10.1142/S1363246905002365.

[63] Petrini L, Maggi C, Priestley MJN, Calvi GM. Experimental Verification of Viscous Damping Modeling for Inelastic Time History Analyzes, Journal of Earthquake Engineering 2008; 12:S1, 125-145, DOI: 10.1080/13632460801925822.

[64] Sousa R, Almeida JP, Correia AA, Pinho R. Shake table blind prediction tests: Contributions for improved fiber-based frame modelling, Journal of Earthquake Engineering 2020, 24:9, 1435-1476, DOI: 10.1080/13632469.2018.1466743.

[65] Correia AA, Almeida JP, Pinho R. Seismic Energy Dissipation in Inelastic Frames: Understanding State-of-the-Practice Damping Models, Structural Engineering International 2013, 23:2, 148-158, DOI: 10.2749/101686613X13439149157001.

[66] Mazzoni S, McKenna F, Scott MH, Fenves GL, Jeremic B. OpenSEES command language manual. Pacific Earthquake Engineering Research Center, University of California, Berkeley, 2003.

[67] Ambraseys N, Smit P, Sigbjornsson R, Suhadolc P, Margaris B. Internet-Site for European Strong-Motion Data, European Commission, Research-Directorate General, Environment and Climate Programme, 2002.

[68] Iervolino I, Galasso C, Cosenza E. REXEL: computer aided record selection for code-based seismic structural analysis, Bulletin of Earthquake Engineering 2010;8:339-362; https://doi.org/10.1007/s10518-009-9146-1.

[69] Gandelli E, Quaglini V, Dubini P, Limongelli MP, Capolongo S. Seismic isolation retrofit of hospital buildings with focus on non-structural components. International Journal of Earthquake Engineering 2018, 35(4), 20-56.